vessel counts. However, our study addressed the biological relevance of neoangiogenesis in the context of lymph node metastasis. We believe our findings are striking enough to require a small sample size to achieve statistical significance.

We take note of studies on CD105 (endoglin) as a marker for angiogenesis. It would be worthwhile to investigate the relationship between CD105 staining and double staining for endothelial markers and proliferation markers.[6]

We are rather surprised at Reis-Filho *et al.*'s comment on exclusion of vessels with thick smooth muscle coats from vessel counting. We wish to quote the methods as stated by Weidner *et al.*: 'Microvessel density was assessed ....; areas of invasive tumour containing the most capillaries and small venules ....'.[2] Vessels with thick smooth muscle coats are unlikely to represent capillaries or small venules.

The Edvin categories are conceptually exciting, but do not appear to be relevant to our study. Our study did not evaluate any predictive or prognostic aspects. The question we addressed was 'whether angiogenesis was essential for the growth of tumour cells after they had metastasized to the lymph nodes'.[7]

Reis-Filho *et al.*'s comments on angiogenic factors reaching non-metastatic lymph nodes draining cancers, thereby resulting in higher vessel counts, are thought-provoking. Though theoretically the possibility exists, our results do not support it. The MIB1+ vessel count was extremely low in these non-metastatic lymph nodes, thereby suggesting a lack of appreciable neoangiogenesis. Furthermore, MIB1+ vessel counts were similar in non-metastatic lymph nodes and in 'normal' mucosae adjacent to the primary tumours.[1]

K N Naresh
A M Borges

Department of Pathology, Tata Memorial Hospital, Mumbai, India

1. Naresh KN, Nerurkar AY, Borges AM. Angiogenesis is redundant for tumour growth in lymph node metastases. *Histopathology* 2001; 38; 466–470.
2. Weidner N, Semple JP, Welch WR, Folkman J. Tumor angiogenesis and metastasis—correlation in invasive breast carcinoma. *N. Engl. J. Med.* 1991; 324; 1–8.
3. Fox SB. Tumour angiogenesis and prognosis. *Histopathology* 1997; 30; 294–301.
4. Weidner N, Folkman J, Pozza F *et al.* Tumor angiogenesis: a new significant and independent prognostic indicator in early-stage breast carcinoma. *J. Natl. Cancer Inst.* 1992; 84; 1875–1887.
5. Eberhard A, Kahlert S, Goede V, Hemmerlein B, Plate KH, Augustin HG. Heterogeneity of angiogenesis and blood vessel maturation in human tumors: implications for antiangiogenic tumor therapies. *Cancer Res.* 2000; 60; 1388–1393.
6. Kumar S, Ghellal A, Li C, Byrne G, Haboubi N, Wang JM, Bundred N. Breast carcinoma: vascular density determined using CD105 antibody correlates with tumor prognosis. *Cancer Res.* 1999; 59; 856–861.
7. Giatromanolaki A, Koukourakis MI, Sivridis E, O'Byrne K, Gatter KC, Harris AL. 'Invading edge vs. inner' (edvin) patterns of vascularization: an interplay between angiogenic and vascular survival factors defines the clinical behaviour of non-small cell lung cancer. *J. Pathol.* 2000; 192; 140–149.

Lack of angiogenesis in lymph node metastases of carcinomas is growth pattern-dependent

Sir: We have read with great interest the paper of Naresh *et al.*,[1] in the May 2001 issue of *Histopathology*, describing the redundancy of anglogenesis for tumour growth in lymph node metastases of head and neck squamous cell carcinomas. The conclusions of the investigators are based on the lower microvessel density in metastatic lymph nodes compared with non-metastatic lymph nodes and on the lower fraction of microvessels with proliferating endothelial cells in metastatic lymph nodes compared with the respective primary tumours.

Exceptions to the 'Folkman-hypothesis', that solid tumours need angiogenesis to grow,[2] are being reported with increasing frequency. In the experimental glioblastoma model of Holash *et al.* tumours initially grow by co-opting the vasculature which surrounds the tumour cell colony, until a kind of suicidal reaction of the pre-existing vessels occurs, leading to hypoxia and subsequent angiogenesis.[3] These observations imply that tumour cells are capable of conserving, and not destroying, the host-derived stroma. Given the vast amount of data concerning the proteolytic nature of invasive tumour cells and the presence of desmoplastic stroma in many tumours, this respect for the pre-existing stroma is not warranted. We therefore argued that not all primary or metastatic tumours would be capable of initial co-option or of parasitism, i.e. prolonged co-option beyond the initial growth phase. In primary non-small-cell lung tumours different growth patterns were indeed observed, of which one was designated as putatively angiogenesis-independent.[4]

We have investigated the growth patterns of liver metastases of adenocarcinomas of colon and breast cancer and found one growth pattern, the 'replacement' pattern, in which hepatocytes were replaced by

tumour cells without disruption of the stromal architecture of the liver.[5] The co-opted sinusoidal microvessels did not express CD34, a marker present on nearly all blood vessels in the primary tumours, but not on normal sinusoidal liver blood vessels. Endothelial cell proliferation was very low in this type of metastases and the ratio of tumour cell proliferation to endothelial cell proliferation, roughly reflecting the degree of angiogenesis-independent growth, was high compared with the other growth patterns.

Our hypothesis is that lymph node metastases of carcinomas are also a heterogeneous group of tumours showing growth patterns with distinct angiogenic profiles. This can be partly deduced from the overlap of the 95% confidence interval for the mean of the MIB-1-positive vessel count between the group of metastatic lymph nodes (0.6–2.4) and the group of primary tumours (1.7–5) in Table 2 of the paper of Naresh *et al.*

Two primary ductal breast carcinomas of patients with lymph node metastases were taken from our archives. One tumour had an infiltrative growth pattern, conserving pre-existing epithelial and stromal structures within the tumour. The other tumour had an expansive growth pattern, pushing aside these structures. In all the lymph node metastases of the former tumour, the lymph node architecture was conserved at the interphase between the tumour and the lymphoid tissue, as demonstrated by a reticulin stain (Figure 1a,b). The fraction of blood vessels with proliferating endothelial cells, counted at the

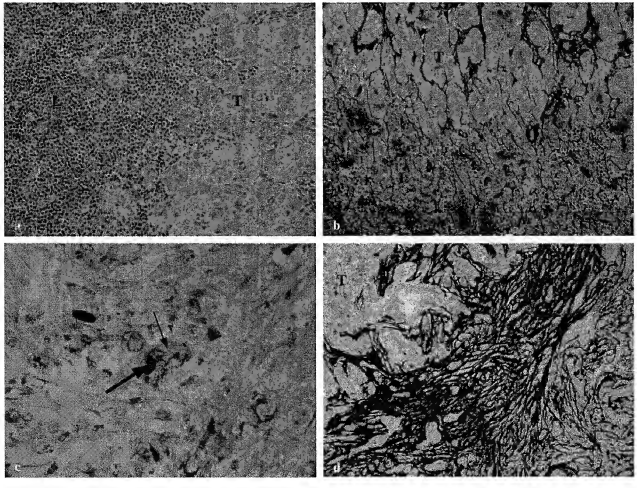

Figure 1. a, Haematoxylin and eosin stain of a lymph node metastasis of a ductal breast carcinoma with an infiltrative growth pattern (T, tumour; L, lymphoid tissue). b, Reticulin stain of the same metastasis: the tissue architecture of the lymph node is conserved at the interphase between tumour and lymphoid tissue. c, Double immunostaining against Ki67 (brown) and CD31 (red): the broad arrow indicates a proliferating endothelial cell. The small arrow indicates a resting endothelial cell. d, Reticulin stain of a metastasis of a ductal breast carcinoma with an expansive growth pattern. A broad desmoplastic ring separates the tumour (T) from the lymphoid tissue (L).

interphase after double immunostaining for Ki67 and CD31, was 1.6% ($n = 1$; Figure 1c). Microvessel density was 14.4 vessels/field (magnification ×400). In contrast, all the lymph node metastases of the latter tumour formed a nodule that was separated from the lymphoid tissue by a broad desmoplastic rim. The lymph node architecture was not conserved at the interphase between tumour and lymphoid tissue (Figure 1d). The fraction of blood vessels with proliferating endothelial cells counted at the interphase was 5.6%. Microvessel density was 12.4 vessels/field. The investigated metastases were of comparable size.

These preliminary observations suggest that the degree of angiogenesis-(in)dependent growth of lymph node metastases is determined by their growth pattern, as has been shown by us to be the case for liver and skin metastases of colorectal and breast carcinomas.[5,6] Prediction of the growth pattern of metastases by analysing the primary tumour might become important in clinical oncology since these growth patterns might have distinct responses to cytotoxic and anti-angiogenic treatment. Mechanisms responsible for the differences in growth pattern need to be elucidated.

P B Vermeulen
P Sardari Nia
C Colpaert
L Y Dirix
E Van Marck

Department of Pathology, University Hospital Antwerp, Edegem and Angiogenesis Group, St. Augustinus General Hospital, Wilrijk, Belgium

1. Naresh KN, Nerurkar AY, Borges AM. Angiogenesis is redundant for tumour growth in lymph node metastases. *Histopathology* 2001; 38; 466–470.
2. Folkman J. What is the evidence that tumors are angiogenesis dependent? *J Natl Cancer Inst* 1990; 82; 4–6.
3. Holash J, Wiegand SJ, Yancopoulos GD. New model of tumor angiogenesis: dynamic balance between vessel regression and growth mediated by angiopoietins and VEGF. *Oncogene* 1999; 18; 5356–5362.
4. Pezzella F, Pastorini U, Tagliabue E *et al.* Non-small-cell lung carcinoma tumor growth without morphological evidence of neoangiogenesis. *Am J Pathol* 1997; 151; 1417–1423.
5. Vermeulen PB, Colpaert C, Salgado R *et al.* Liver metastases from colorectal adenocarcinomas grow in three patterns with different angiogenesis and desmoplasia. *J Pathol* 2001; 195; 336–342.
6. Colpaert C, Vermeulen P, Lachaert R, van Beest P, Govaerts G, Dirix L, Van Marck E. Cutaneous breast cancer deposits show distinct growth patterns with different degrees of angiogenesis and fibrin deposition. (submitted).

bcl-2 and p21 immunostaining of cervical tubo-endometrial metaplasia

Sir: We read with interest the recent correspondence in *Histopathology* from Dr Piek and colleagues regarding the expression in the normal fallopian tube of some common differentiation and proliferation proteins.[1] These authors showed that bcl-2 was highly expressed in the cytoplasm of secretory cells, whereas ciliated cells were completely negative. Conversely, p21 was often expressed in the nuclei of ciliated cells, whereas secretory cells were usually negative. The authors concluded that this pointed to a role for p21 and bcl-2 in the differentiation of ciliated and secretory cells, respectively, in the fallopian tube.

In a previous study we investigated the immunohistochemical detection of p53 and bcl-2 proteins in a variety of neoplastic and non-neoplastic endocervical glandular lesions and showed that there was diffuse positive staining for bcl-2 in most cases of cervical tubo-endometrial metaplasia.[2] The findings of Dr Piek and colleagues prompted us to carry out a further small study investigating bcl-2 and p21 immunostaining in 10 cervices showing tubo-endometrial metaplasia, a commonly encountered lesion in the cervix, especially following cone biopsy or some other procedure.[3,4] Diffuse cytoplasmic positivity was found in all cases of tubo-endometrial metaplasia (Figure 1), but there was no staining of normal endocervical glands. Furthermore, on morphological examination of haematoxylin and eosin-stained slides we could not distinguish ciliated from secretory cells, as can be done in the normal fallopian tube. In most cases, the vast majority of the cells were ciliated and in other cases there were areas composed of ciliated cells interspersed with areas of non-ciliated cells. However, apart from the presence

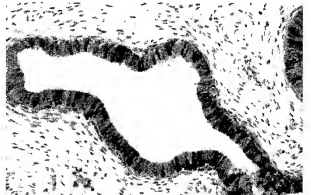

Figure 1. Diffuse strong cytoplasmic positivity for bcl-2 in tubo-endometrial metaplasia.

American Journal of Pathology, Vol. 155, No. 3, September 1999

Vascular Channel Formation by Human Melanoma Cells *in Vivo* and *in Vitro*: Vasculogenic Mimicry

Andrew J. Maniotis,*† Robert Folberg,†‡§ Angela Hess,* Elisabeth A. Seftor,*† Lynn M.G. Gardner,‡ Jacob Pe'er,¶ Jeffrey M. Trent,‖ Paul S. Meltzer,‖ and Mary J. C. Hendrix*†

From the Departments of Anatomy and Cell Biology, University of Iowa Cancer Center,† and the Departments of Ophthalmology and Visual Sciences‡ and Pathology,§ University of Iowa College of Medicine, Iowa City, Iowa; the Department of Ophthalmology,¶ Hadassah University Hospital, Jerusalem, Israel; and the Cancer Genetics Branch, National Human Genome Research Institute, National Institutes of Health, Bethesda, Maryland‖*

Tissue sections from aggressive human intraocular (uveal) and metastatic cutaneous melanomas generally lack evidence of significant necrosis and contain patterned networks of interconnected loops of extracellular matrix. The matrix that forms these loops or networks may be solid or hollow. Red blood cells have been detected within the hollow channel components of this patterned matrix histologically, and these vascular channel networks have been detected in human tumors angiographically. Endothelial cells were not identified within these matrix-embedded channels by light microscopy, by transmission electron microscopy, or by using an immunohistochemical panel of endothelial cell markers (Factor VIII-related antigen, Ulex, CD31, CD34, and KDR[Flk-1]). Highly invasive primary and metastatic human melanoma cells formed patterned solid and hollow matrix channels (seen in tissue sections of aggressive primary and metastatic human melanomas) in three-dimensional cultures containing Matrigel or dilute Type I collagen, without endothelial cells or fibroblasts. These tumor cell-generated patterned channels conducted dye, highlighting looping patterns visualized angiographically in human tumors. Neither normal melanocytes nor poorly invasive melanoma cells generated these patterned channels *in vitro* under identical culture conditions, even after the addition of conditioned medium from metastatic pattern-forming melanoma cells, soluble growth factors, or regimes of hypoxia. Highly invasive and metastatic human melanoma cells, but not poorly invasive melanoma cells, contracted and remodeled floating hydrated gels, providing a biomechanical explanation for the generation of microvessels *in vitro*. cDNA microarray analysis of highly invasive *versus* poorly invasive melanoma tumor cells confirmed a genetic reversion to a pluripotent embryonic-like genotype in the highly aggressive melanoma cells. These observations strongly suggest that aggressive melanoma cells may generate vascular channels that facilitate tumor perfusion independent of tumor angiogenesis. *(Am J Pathol 1999, 155:739–752)*

It is generally assumed that tumors require a blood supply for growth and metastasis.[1] The development of the tumor microcirculation compartment includes both the production of new blood vessels (angiogenesis) and their remodeling.[2] In fact, the number of vessels[3] and the patterning of the microcirculation[4] by remodeling events are used as histological markers of tumor progression. Although attention has been focused on factors that stimulate and suppress tumor angiogenesis, the molecular mechanisms underlying tumor remodeling remain enigmatic. It is therefore critical to investigate remodeling of the intratumoral microvasculature in various tumor models.

Melanoma is among the better characterized tumor models with respect to prognostic staging of disease progression. The rising incidence of cutaneous melanoma makes this tumor an important public health problem. Melanoma of the interior of the eye, uveal melanoma, although much less common than cutaneous melanoma, poses a threat to vision and significant morbidity; nearly 50% of patients with uveal melanoma die from metastatic melanoma.[5] Cutaneous melanoma may disseminate through lymphatics or blood vessels. In contrast, the interior of the eye lacks lymphatics, and uveal melanoma, which develops in one of the most capillary-rich tissues of the body, is a paradigm for pure hematogeneous dissemination of cancer.[6] Therefore, the development of a tumor microcirculation in uveal melanoma is a rate-limiting step for hematological metastasis and serves as an important model for study of the cellular and molecular infrastruc-

Supported by the University of Iowa Central Microscopy Research Facility, the Charles Hendrix Research Foundation, and the University of Iowa Leading Woman Scientist Endowment (to M. J. C. H.), by National Institutes of Health Grants R01 CA59702 (to M. J. C. H.), R01 CA80318 (to M. J. C. H. and R. F.), and R01 EY10457 (to R. F.), and in part by an unrestricted grant from Research to Prevent Blindness, Inc. R. F. is a Research to Prevent Blindness Senior Scientific Investigator.

Accepted for publication June 30, 1999.

Address reprint requests to Dr. Mary J. C. Hendrix, Department of Anatomy and Cell Biology, College of Medicine, University of Iowa, Iowa City, Iowa 52242-1109. E-mail: mary-hendrix@uiowa.edu.

ture of the melanoma microvasculature, isolated from the influence of a concomitant lymphatic circulation.

The objective of this investigation was to elucidate the relationship between the aggressive melanoma cell phenotype and the mechanisms responsible for the generation of uniquely patterned matrix-associated vascular channels characteristic of both aggressive human uveal and cutaneous melanomas.

Materials and Methods

Light Microscopy

To highlight the matrix-associated vascular channels of uveal melanomas, tissues were stained with periodic acid-Schiff (PAS), omitting hematoxylin counterstaining to reduce visual noise; black and white photography with a green filter (or the selection of the green channel for digital photography) further highlighted the PAS-positive patterns.[7] Failure to eliminate hematoxylin counterstaining to the PAS stain has resulted in a 50% reduction in the histological detection of PAS-positive looping patterns and networks.[8]

The prognostic significance of the presence of PAS-positive patterns in uveal melanoma was tested by us on a series of 234 patients whose eyes had been removed for uveal melanoma. Details concerning the composition of patients in this data set and statistical analyses were reported elsewhere. Briefly, the primary outcome variables were the time to death from metastatic melanoma or from other causes and the time to follow-up for those patients who were still alive. The analyses focused on time to death from metastatic melanoma. We treated time to death from other causes, time to follow-up for living patients, and time to last contact for patients reported as lost to follow-up as censored times in the data analyses.[4,9,10]

Correlations with Indocyanine Green Angiography

A series of 18 patients with choroidal melanoma were studied prospectively with indocyanine green angiography using a confocal scanning laser ophthalmoscope (Heidelberg Retinal Angiograph, Heidelberg Engineering, Heidelberg, Germany)[11–13]; two of these patients had their eyes removed following the angiogram. The eyes were fixed in 10% neutral buffered formalin for at least 48 hours, and opened via a coronal incision through the pars plana to allow for direct visualization of the tumor surface[14] and to enhance an accurate correlation with retinal landmarks by comparison with pre-enucleation fundus photographs and the confocal angiographs. Each tumor was sectioned through the zone corresponding to the intratumoral microcirculation as seen on the angiograms. Sections were stained using the modified PAS without hematoxylin stain. Details of the prospective study and the angiographic-histological correlations were reported elsewhere.[13]

Transmission Electron Microscopy

Human tissue samples and cultures were fixed initially in 10% neutral buffered formalin. One half of the tumor sample was processed for diagnostic light microscopy and stained with the PAS stain without hematoxylin counterstaining. Areas of tumor containing PAS-positive looping patterns were identified and were used to map and microdissect areas of tumor containing these patterns from wet tissue corresponding to the opposite face of tissue embedded in paraffin. These small regions of tumor were postfixed in 2.5% buffered glutaraldehyde and were postfixed further in a solution of 1% osmium tetroxide, dehydrated, and embedded in a standard fashion. Thin sections were stained with uranyl acetate-lead citrate and examined with a Hitachi S-7000 transmission electron microscope.

Immunohistochemistry

For light microscopic immunohistochemistry, paraffin sections were cut at 4 to 5 μm. Slides were deparaffinized using xylene and absolute ethanol, rinsed in distilled water, exposed to proteinase K for 2 minutes or antigen unmasking. (The antigen unmasking solution was heated in a steamer to 95°C, then cooled to 75°C before slides were placed in it.) The solution and slides were heated in an oven at 65°C for 55 minutes. For Ulex (Vector Laboratories, Burlingame, CA), Factor VIII-related antigen (Dako, Carpenteria, CA), CD31 (Dako), and KDR (Flk-1; Santa Cruz Biotechnology, Santa Cruz, CA), slides were placed in either PBS or Tris-buffered saline, pH 7.4 (TBS, Sigma Chemical Co., St. Louis, MO). The sections were rinsed with phosphate-buffered saline (PBS) and blocked subsequently with 10% normal horse serum in PBS. Sections were stained with the appropriate primary antibody or lectin for 1.5 hours, then incubated for 20 minutes (10 minutes for KDR) with biotinylated anti-rabbit or anti-mouse immunoglobulins in PBS. This was followed by incubation with streptavidin (Zymed, South San Francisco, CA) conjugated to alkaline phosphatase in PBS for 20 minutes, then by a brief rinse in distilled water. Sections were exposed to Vector red chromogen (Vector Laboratories) for up to 2 minutes, an enhancement solution (Zymed) for 5 minutes, rinsed in distilled water, counterstained with Mayer's hematoxylin for 8 minutes, and coverslipped with a permanent mounting medium. For CD34 (Novocastro, Vector Laboratories), antigen unmasking was followed by staining with the CD34 for 30 minutes, washing in Tris buffer, then placement into Envision Polymer (Dako) for 30 minutes and washing with Tris buffer. Sections were exposed to Vector red chromogen for up to 2 minutes, washed in distilled water, counterstained with Mayer's hematoxylin for 8 minutes, and coverslipped with permanent mounting media.

Dual immunofluorescence labeling of keratins 8 and 18 and vimentin IFs was accomplished using antikeratin antibodies CK-5, (Sigma) conjugated with Oregon Green (Molecular Probes, Eugene, OR) for keratins, and V.9 (Dako) conjugated with Texas Red-X (Molecular Probes)

for vimentin, as previously described,[15] All coverslips were observed with either a Zeiss LSM410 (Thornwood, NY) or Bio-Rad (Hercules, CA) 1024 laser scanning confocal microscope, and the images digitized using either the Zeiss KS400 or Bio-Rad Confocal Assistant V. 3.10 software packages.

Dual immunohistochemistry labeling of CD31 and S-100 protein was accomplished using an antibody to CD31 as described above, followed by application of a serum blocking solution (Zymed) for 15 minutes. Sections were then exposed to antibody to S-100 protein (Dako) for 1.75 hours followed by washing with PBS-Tween Gold-conjugated secondary antibody (Zymed) which was diluted by 50% in PBS and applied for 30 minutes. Sections were then washed in PBS-Tween and were exposed to a silver enhancer (Zymed) for 10 minutes, followed by a wash in PBS-Tween. The sections were then counterstained with Mayer's hematoxylin for 8 minutes and coverslipped with permanent mounting medium. These sections were viewed by direct light microscopy to detect CD31 and by epipolarization microscopy to detect the S-100 protein signal.

Cell Culture

Cell lines derived from primary choroidal or ciliary body melanomas or from foci of metastatic uveal melanoma to the liver[16] and normal melanocytes, as described previously,[17] as well as the human cutaneous metastatic melanoma cell line C8161,[18] were maintained in Dulbecco's modified Eagle's medium (DMEM, Life Technologies, Gaithersburg, MD) supplemented with 10% fetal bovine serum (FBS, Gemini Bioproducts, Calabasas, CA).[19] Endothelial cells derived from pulmonary, brain, and dermal microvasculature (HMEC-1), HUVECs, and embryonic chick endothelial cells were maintained in DMEM, 20% FBS, or 1× MITO+ (Collaborative Biomedical, Bedford, MA).[20,21] Cell cultures were determined to be free of mycoplasma contamination using the GenProbe rapid detection system (Fisher, Itasca, IL).

Three-Dimensional Cultures

Twelve microliters of Matrigel or Type I collagen (Collaborative Biomedical) were dropped onto glass coverslips and allowed to polymerize for 1 hour at 37°C. Tumor cell lines, normal uveal melanocytes, or endothelial cells were then seeded on top of the gels at high density and allowed to incubate. For conditioned media experiments, media were collected and passaged through a 0.2-μm filter before being placed on the appropriate cells. Addition of conditioned media-soluble factors (basic fibroblast growth factor (bFGF), transforming growth factor (TGF)-β, vascular endothelial growth factor (VEGF), platelet-derived growth factor (PDGF), and tumor necrosis factor (TNF)-α, all from Sigma) or antibodies to $\alpha_v\beta_3$ or α_v (Chemicon, Temecula, CA) was performed by pretreatment and continuous treatment regimes during the 1- to 2-week incubation period in 3D cultures (Table 1).

Invasion Assay

Tumor cells (1×10^5) were seeded into the upper wells of the MICS (membrane invasion culture system) chamber[22] onto collagen/laminin/gelatin-coated (Sigma) polycarbonate membranes containing 10-μm pores (Osmonics, Livermore, CA) in DMEM containing 1× MITO+ (Collaborative Biochemical). After 24 hours of incubation at 37°C, the cells that invaded each membrane were collected, stained, and counted as previously described.[23] Percent invasion was corrected for proliferation and calculated as follows:

$$\frac{\text{total number of invading cells}}{\text{total number of cells seeded}} \times 100$$

Micromanipulation and Microinjection

For micromanipulation, an Eppendorf workstation was used with a second Leitz manipulator, and morphological alterations were quantitatively recorded with a video recording device and measured with NIH Image software.[24] For microinjections, Texas Red (Molecular Probes) was preloaded into short barrel pipettes pulled on a Sutter pipette puller, delivered into large sinusoidal channels, and observed continuously for 30 minutes.

In Vitro *Collagen Lattice Deformation Assays*

Floating collagen lattices[25] were prepared by placing a 250-μl drop of the collagen-cell suspension (0.65 mg/ml of Collagen I (Collaborative Biomedical) and 1.25×10^5 cells/ml) in a bacteriological 35-mm Petri dishes to prevent adhesion of the gel to the culture substrate. After 1 hour at 37°C to allow polymerization of the collagen, 1.6 ml of complete medium was placed over the collagen lattice. Lattice contraction was quantified as the relative change in the gel diameter over time, using NIH Image software. Rhodamine 123 dye (Molecular Probes) was incubated with melanoma cells for 18 hours and washed before cells were placed on floating gels to demonstrate the distribution of tumor cells in contracting gels.

Microarray Analysis

cDNA microarrays detected altered gene expression in highly invasive melanoma cells by a method previously described.[26] Relative expression of selected genes critical for vascular channel formation is reported (Table 2) as highly invasive and metastatic *versus* poorly invasive uveal melanoma cells. Hybridization to cDNA microarrays followed the previously described procedures[27] (see also http://www.nhgri.nih.gov/DIR/LCG/15K/HTML/). Briefly, RNA extracted from poorly invasive and highly invasive/metastatic melanoma cells was converted to cDNA in the presence of fluorescent nucleotides Cy3- or Cy5-dUTP. The labeled cDNA pools were mixed and hybridized to microarrays containing 5000 cDNA elements selected from the Unigene database.[28] Fluorescence intensities for each gene were measured with a

custom instrument, and ratios were calculated as described.[27]

Results

Histology of the Melanoma Microcirculation, its Prognostic Significance, and in Vivo Functional Correlations

Many melanomas enlarge within the uvea without containing prominent zones of necrosis (Figure 1A). In our series of 234 eyes removed for malignant melanoma of the choroid or ciliary body, we discovered that 106 (45%) tumors contained networks of interconnected PAS-positive back-to-back loops (Figure 1B).[4] Uveal melanoma tends to spread first and preferentially to the liver,[29] and we discovered that liver metastases from uveal melanomas also contained these patterns (Figure 1C), as did foci of metastatic uveal melanoma in other organ sites.[16] We have also detected PAS-positive loops and networks in metastatic cutaneous melanoma (Figure 1D).

By conventional hematoxylin-eosin stains and with high magnification, the PAS-positive loops were seen to have a solid component in some areas which splayed open to reveal hollow channels, some of which contained red blood cells; these channels also connected to somewhat larger vascular spaces containing red blood cells (Figure 1E). Light microscopy revealed that the interior of these hollow channels, red blood cell-containing channels, and vascular spaces was not lined by an endothelium.

We studied the prognostic significance of the PAS-positive patterned matrix-associated vascular channels in a group of 234 patients whose eyes were removed for uveal melanoma. The histological presence of loops or networks had a stronger association with death from metastatic melanoma, in a multivariate Cox proportional hazards model, than all other conventional histological features studied, including tumor size, cell type, and mitotic activity.[4,9,10] There was a strong statistical separation in survival between patients whose tumors lacked loops and networks and those whose tumors contained these patterns (Figure 1F). The statistical association between the histological presence of microcirculatory loops and networks and death from metastatic melanoma has been confirmed by independent laboratories.[8,30,31] We found subsequently that loops and networks are not found in uveal nevi,[32] that networks tend to localize preferentially to the periphery of the tumor (the tumor growth zone),[33] that the amount of tumor remodeling by looping patterns (the percentage of area occupied by these patterns on a two-dimensional tissue section) had a negative effect on patient survival,[10] and that the classification of tumors into high- and low-risk for metastasis was likely to be consistent regardless of the tissue plane sampled within a large tumor.[34]

These PAS-positive patterns were presumed to be associated with the tumor microcirculation for several reasons. First, PAS-positive patterns connect in tissue sections with vascular spaces containing red blood cells (Figure 1, B and C). Second, PAS-positive networks were traced in serial sections to connect with the vortex vein, which drains the choroid.[6] Third, the patterns splay open and contain red blood cells (Figure 1E). Fourth, comparisons of adjacent tissue sections stained alternately with PAS and with Ulex europaeus agglutinin I showed histological correspondence between PAS-positive patterns with Ulex staining.[7] Finally, three-dimensional reconstructions by laser scanning confocal microscopy of thick melanoma tissue sections stained with Ulex revealed anastomosing tubular and sinusoidal structures, consistent with vascular channels.[6,35]

The ability to directly visualize the circulation of blood in a tumor in the absence of lymphatics makes the angiographic study of intraocular melanoma an ideal venue for investigating the functional perfusion of the patterned matrix-associated vascular channels in patients. Two patients from a series of 18 patients whose uveal melanomas were imaged clinically with this technique had their eyes removed after confocal angiography. One of these patients showed angiographic evidence of loops forming networks within the tumor (Figure 1G), and we detected PAS-positive network patterns in histological sections taken from this area of the tumor (Figure 1H). The other patient had angiographic evidence of only large, pre-existing choroidal vessels within the tumor (an absence of loops, Figure 1I) and showed only normal choroidal vessels histologically and no looping patterns (Figure 1J).[13] Unlike cutaneous melanoma, which is usually accessible to biopsy without major morbidity, it is difficult to obtain representative quantities of tumor tissue from within the eye for histopathological analysis without risking compromise to vision. Thus, the ability of ophthalmologists to image prognostically significant microcirculatory patterns clinically in patients by confocal angiography or by ultrasound power spectrum analysis[36] provides noninvasive substitutes for biopsy.

Transmission Electron Microscopy of Melanoma Microcirculation Patterns

By light microscopy, patterned matrix-associated vascular channels containing red blood cells did not appear to be lined by endothelium. We therefore microdissected tissue sections from uveal melanomas to isolate tumor tissue containing PAS-positive loops and networks of loops (Figure 2A). Ultrastructurally, these vascular channels were not lined by endothelium but were delimited by a thin basal lamina and were lined externally by tumor cells (Figure 2B) containing premelanosomes and melanosomes (Figure 2C). These ultrastructural findings confirmed the light microscopic observations that melanoma cells were associated with these vascular channels and were situated on the outer surface of the tubular wall (Figure 2D) rather than internal, as would be expected of an endothelial lining. The presence of a basal lamina lining the vessel wall correlated with the PAS-positive staining of the patterned matrix in tissue sections. The PAS stain is used routinely in ophthalmic pathology to facilitate identification of critical intraocular basement

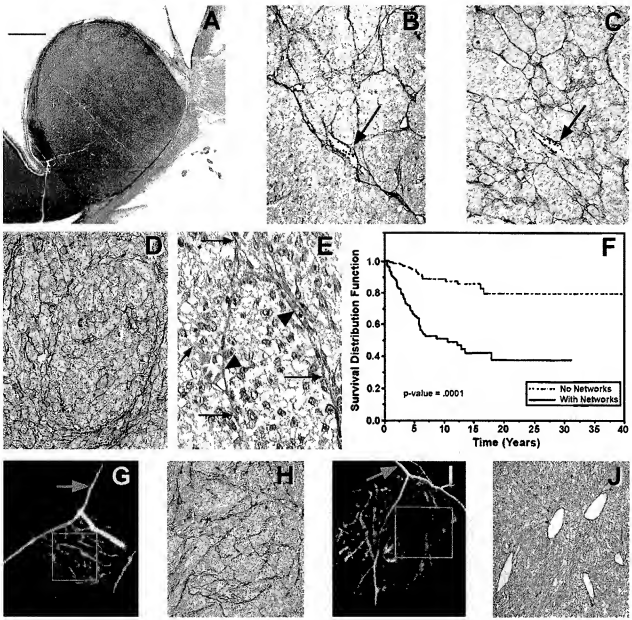

Figure 1. Histology of the melanoma microcirculation, its prognostic significance, and *in vivo* functional correlations. A: Primary uveal melanoma in the choroid of a patient who died of metastatic melanoma 3 years after the eye was removed. Note the absence of necrosis. Hematoxylin-eosin stain; scale bar, 2 mm. B: Light microscopic view of PAS-stained tissue sections of primary human uveal melanoma (arrow demonstrates a sinusoid with red blood cells). C: Uveal melanoma metastatic to the liver, showing patterns of interconnected loops forming networks anastomosing to sinusoids (arrow) containing red blood cells. D: PAS-stained histological section of metastatic cutaneous melanoma containing multiple networks. E: Hematoxylin-eosin stained section of primary uveal melanoma; the structures corresponding to the PAS-positive components of loops and networks consist of solid cords (arrows) that connect to round channels or tubes containing red blood cells (arrowheads). Note that these tubules are lined externally by melanoma cells and no endothelial cells are identified. F: Kaplan-Meier survival curves for deaths from metastatic uveal melanoma: melanomas without networks *versus* melanomas with networks (after Folberg, et al[6]). G: Angiogram of uveal melanoma taken after intravenous injection of indocyanine green and photographed with a laser scanning confocal ophthalmic recording device.[11] The vessels forming an inverted "Y," highlighted by the yellow arrow, are within the retina. The anastomosing loops between the two inverted branches of the "Y" formed by the retinal vessels and enclosed by the yellow box are deeper within the tumor and represent the microcirculation of this melanoma. This eye was subsequently removed and studied histologically[13] (shown in H). H: Tissue section stained by PAS, without hematoxylin counterstain, taken from the tumor at the location enclosed by the box from the angiogram (G). Many PAS-positive loops forming networks are seen in this tissue, corresponding precisely to the loops seen in the angiogram. I: Angiogram of uveal melanoma taken after intravenous injection of indocyanine green and photographed with a laser scanning confocal ophthalmic recording device.[11] In contrast to the angiogram shown in G, looping vessels are not seen within the tumor (yellow box). The vessels within the tumor are parallel straight vessels. This eye was subsequently removed and studied histologically[13] (shown in J). J: Tissue section stained by PAS without hematoxylin taken from the area in the tumor enclosed by the box on the angiogram (I). Dilated normal choroidal vessels are identified and correspond to the straight, parallel vessels on the angiogram. Scale bar, 2 mm (A). Original magnifications, ×40 (B, C, H, J), ×80 (D). ×120 E. Tissue stains: hematoxylin-eosin (A and E), PAS without hematoxylin counterstaining, photographed with a green filter (B-D, H-J).[7]

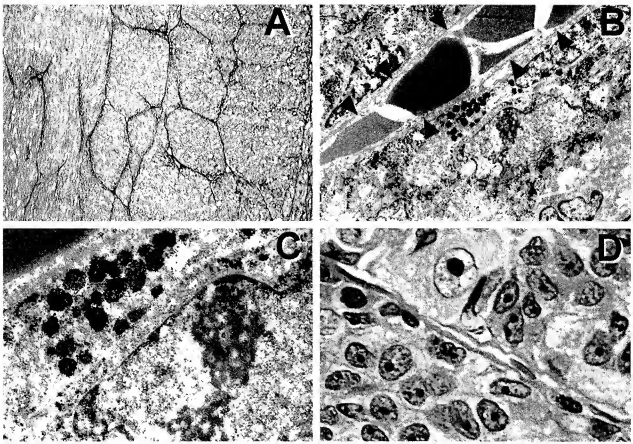

Figure 2. Transmission electron microscopy of melanoma microcirculation patterns. A: Tissue section of primary uveal melanoma stained by PAS without hematoxylin counterstain (same tumor as illustrated in Figure 1E). Areas from this tumor were microdissected and studied by transmission electron microscopy. B: Scanning magnification transmission electron micrograph of a tubule containing a single-file column of red blood cells. This vascular channel is lined by a thin basal lamina (arrowheads) corresponding to the walls of the channel seen by conventional light microscopy. There are no endothelial cells lining the tubule. Tumor cells containing melanosomes and premelanosomes lie external to the basal lamina. C: Higher magnification of Figure 2C illustrating premelanosomes and melanosomes within the tumor. D: Hematoxylin-eosin-stained tissue section of primary uveal melanoma. A vascular channel containing red blood cells is lined externally by tumor cells; endothelial cells are not identified. Original magnifications, ×40 (A), ×10,000 (B), ×30,000 (C), ×100 (D).

membrane structures such as Descemet's membrane, Bruch's membrane, and the internal limiting membrane of the retina.

Immunohistochemical Profile of Melanoma Intratumoral Patterned Vascular Channels

We and others had reported previously that it is possible to label PAS-positive patterns with Ulex,[7,35] Factor VIII-related antigen,[6] CD31,[6] and CD34.[31] In light of the absence of demonstrable endothelial cells by light and transmission electron microscopy in the matrix-associated vascular channels, we further evaluated the distribution of endothelial markers within these patterns.

We stained tissue sections of uveal melanomas containing abundant PAS-positive looping patterns and networks for the distribution patterns of Factor VIII-related antigen, Ulex europaeus agglutinin I, CD31, CD34, and KDR. As controls, we used either normal adjacent choroidal vasculature (which includes the fenestrated endothelium of the choriocapillaris), tissue sections of granulation tissue, or tissue sections of proliferative diabetic retinopathy—a classic example of ocular angiogenesis. The vessels of proliferative diabetic retinopathy labeled with endothelial cell markers, such as Factor VIII-related antigen, appeared randomly clustered as discrete channels (Figure 3A) and were clearly lined by endothelial cells (Figure 3B), as demonstrated with hematoxylin counterstaining. These angiogenically derived vascular structures of proliferative diabetic retinopathy are quite different from the patterned, interconnected, looping PAS-positive channels found within aggressive melanomas (Figure 3C).

Within a given tumor, staining for endothelial cell markers such as Factor VIII-related antigen (Figure 3D) or CD31 (Figure 3E) was weak, focal, and discontinuous along the patterns, frequently leaving most of the patterns unlabeled. By contrast, the normal vessels of the surrounding choroid labeled consistently with these markers and served as an internal positive control for endothelial cells.

In portions of the patterns that failed to stain with endothelial cell markers, we frequently identified hollow tubes. Some endothelial cell markers, such as CD31, unexpectedly stained tumor cells in the vicinity of patterned tubes (Figure 3F). At high magnification, markers

Table 1. Effects of Conditioned Media and Soluble Factors on Formation of Vessels by Human Uveal Melanoma Cells

Culture designation	Cell phenotype vimentin/keratin IFs	Invasive potential	Added conditioned media (CM)/soluble factors	Vessel formation
UMEL-1 (normal choroid)	+/−	Poor (0.9 ± 0.008)	Without CM	−
			With C918 CM	−
OCM-1A (primary)	+/−	Poor (2.2 ± 0.09)	Without CM	−
			With C918 CM	−
			With M619 CM	−
			With MUM-2B CM	−
			With bFGF, TGF-β, VEGF, PDGF	−
C918 (primary)	+/+	High (12.9 ± 0.31)	Without CM	+
			With UMEL-1 CM	+
			With OCM-1A CM	+
M619 (primary)	+/+	High (12.7 ± 0.4)	Without CM	+
MUM-2B (metastasis)	+/+	High (13.3 ± 0.6)	Without CM	+

Scoring of tumor cell phenotype using classical pathology markers of vimentin (mesenchymal) and cytokeratins 8 and 18 (epithelial) intermediate filaments (IFs) was based on a positive (+) and negative (−) ranking system, determined by immunohistochemistry and/or Northern blot analysis. Invasiveness was calculated as the percentage of cells capable of invading a collagenous matrix-coated polycarbonate membrane over 24 hours within a membrane invasion culture system (MICS) compared with the total number of cells seeded (± SE; $n = 6$ wells per measurement and run in duplicate experiments). Conditioned media (CM)/soluble factors experiments were performed by treating designated 3D cultures of cells with CM from specific cell lines or exogenously added factors for 1 to 2 weeks *in vitro*, followed by microscopic scoring of vascular tube formation on 3D Matrigel or on Type I collagen gels.

such as Factor VIII-related antigen that stained the patterns were clearly seen to label the interior of the hollow lumen segmentally (Figure 3G), perhaps accounting for the discontinuous labeling seen in lower magnification (Figure 3D). We also noted that staining for endothelial cell markers such as Ulex (Figure 3H), CD34 (Figure 3I), and KDR (Figure 3J) stained the lumen contents around red blood cells within the patterns. Furthermore, when endothelial markers stained the lumen contents of the patterns, they did not stain the lumen wall, and endothelial cell nuclei were not identified within the tubes by hematoxylin counterstaining.

After double-labeling a tissue section of primary uveal melanoma with both CD31 and S-100 protein, we again did not detect staining of most of the patterns with CD31 (Figure 3K), but we did observe intense staining of cells external to the lumen of the patterned channels with S-100 protein (staining for S-100 protein is characteristic of and consistent with melanoma cells, but not with vascular endothelium; Figure 3L). In fact, staining for S-100 protein was so intense that the tumor cells outlined the negatively labeled lumen of the patterned channels (Figure 3L).

Therefore, by conventional light microscopy, transmission electron microscopy, and an immunohistochemical panel of endothelial cell markers, the looping patterned matrix-associated vascular channels of aggressive melanomas were not found to be lined by vascular endothelium.

In Vitro *Reconstitution of Patterned Matrix-Associated Vascular Channels by Cultured Aggressive Melanoma Cells*

The absence of endothelial cells lining the patterned matrix-associated vascular channels of aggressive and metastatic melanomas suggested that the melanoma cell phenotype might play a role in the generation of these patterns. To test this hypothesis, we examined the capacity of melanoma cells of varying invasive and metastatic potential to recapitulate *in vitro* the network patterns seen in tissue sections in the absence of endothelial cells and fibroblasts.

Human cultures of the highly invasive M619 (Figure 4A) and C918 uveal melanoma cells, metastatic MUM-2B uveal melanoma cells (Figure 4B), and C8161 metastatic cutaneous melanoma cells (Figure 4C), all reconstituted with extraordinary fidelity the architectural patterns of loops and networks *in vitro* in gels containing Matrigel (Figure 4, A and C) or dilute Type I collagen (Figure 4B). These observations were specific for the aggressive melanoma cell phenotype, because poorly invasive OCM-1A uveal melanoma cells and normal UMEL-1 cells failed to form vessel networks *in vitro* under identical culture conditions on either Matrigel (Figure 4D) or dilute Type I collagen (Figure 4E). As in patient tissue samples, these *in vitro* tumor cell-generated patterned vascular channels were PAS-positive.

We asked whether this pattern formation was induced by a factor secreted in the conditioned medium. Addition of conditioned media from the highly invasive and metastatic cell lines (M619, C918, MUM-2B) to poorly invasive cells (OCM-1A, UMEL-1) did not result in patterned vascular channel formation (Table 1). Moreover, basic fibroblast growth factor (bFGF), transforming growth factor (TGF)-β, vascular endothelial growth factor (VEGF), platelet-derived growth factor (PDGF), and tumor necrosis factor (TNF)-α, tested individually or in combination, failed to induce formation of these networks when added to cultures of the poorly invasive cells. Similarly, no vascular channels were formed in <2% hypoxic conditions. Conversely, conditioned media from poorly invasive cells failed to inhibit *in vitro* vessel formation by highly invasive cells. Furthermore, commercially available blocking antibodies raised against $\alpha_v\beta_3$ or the α_v subunit did not inhibit patterned channel formation even at concentra-

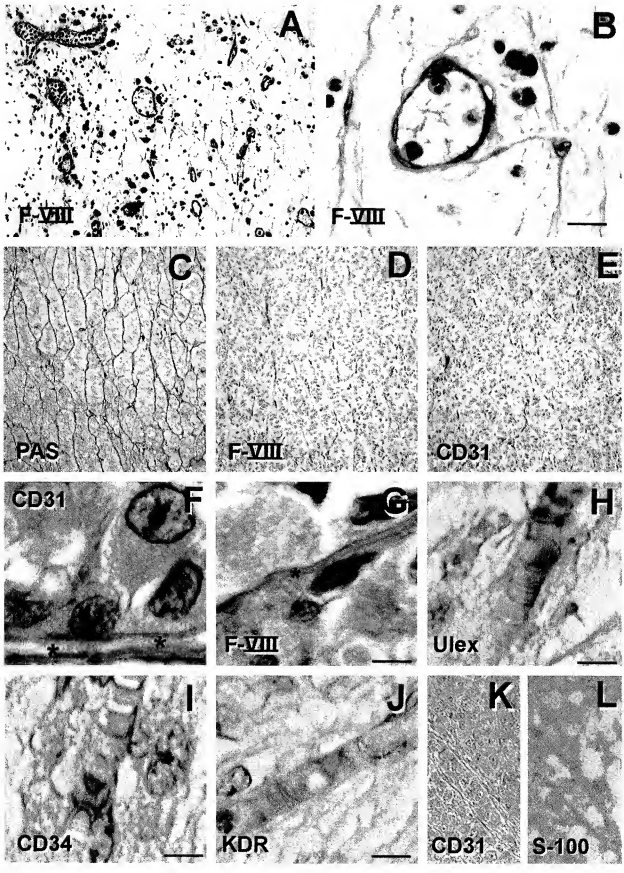
A
F-VIII
B
F-VIII
C
PAS
D
F-VIII
E
CD31
CD31
F
G
F-VIII
H
Ulex
I
CD34
J
KDR
K
CD31
L
S-100

tions exceeding a 1:20 dilution of the antibodies in culture media.

The vascular patterns formed *in vitro* (Figure 4, A-C) compartmentalized spheroidal nests of tumor cells in a fashion identical to spheroidal tumor cell nests delimited by PAS-positive microvessels observed in tissue sections from primary and metastatic melanomas (compare Figure 1, B, C, and D, with Figure 4, A-C). The structures that delimit nests of tumor cells *in vitro* are both sinusoidal and tubular, as demonstrated by histological cross-section of the cultures (Figure 4F).

We tested the perfusion characteristics of patterned tubular and sinusoidal channels generated by melanoma cells *in vitro* with the microinjection of dye into the sinusoids of mature cultures (>2 weeks). Many of these tumor-generated channels were capable of holding the injected dye and distributing it over considerable distances through the *in vitro* generated networks (Figure 4, G and H), reminiscent of the angiographic patterns seen in patients with indocyanine green angiography (Figure 1G).

Biomechanical Potential of Highly Invasive and Poorly Invasive Melanoma Cells

The invasive and metastatic uveal melanoma cell-generated patterns consisted of a phase microscopic acellular translucent tubular network embedded in the underlying cell monolayer (Figure 5A), as demonstrated by direct microdissection (Figure 5B). These channels and sinusoids evolved dynamically and anastomosed within the monolayer over a 3-day to 3-week period. Also, these networks in young cultures encircled subpopulations of tumor cells and varied widely in lumen diameter. By comparison, endothelial cell cords *in vitro* typically demonstrate a more uniform diameter on most matrices[37–40] and most, if not all, of the cultured endothelial cells typically participate in cord formation under identical media and matrix conditions without encircling subpopulations of endothelial cells (Figure 5C). The presence of spheroidal cell nests within the boundaries formed by tumor cell cords is not a characteristic feature of endothelial cord formation in Matrigel or on other matrices (compare Figure 5A with Figure 5C). Therefore, the presence of spheroidal nests of melanoma cells encircled by patterned, acellular hollow tubes in pure tumor cultures constitutes a major difference between tumor and endothelial cord formation under identical conditions.

The potential of many cell types to generate cords, tessellations, and tube-like structures *in vitro* has been linked to their ability to constrict and remodel matrix fibers.[38,41] In addition, highly invasive melanoma cells have been demonstrated to contract floating collagen gels.[42] Because we observed that highly invasive melanoma cells could generate patterned vessels *in vitro*, we explored the ability of these cells to contract floating matrices as evidence of their matrix remodeling potential.

First, we compared the ability of cultured melanoma cells of varying phenotypes with that of endothelial cells to contract gels during similar time periods with identical gel densities and media conditions. Endothelial cells contracted floating collagen gels within 48 hours (Figure 5D). Highly invasive C918 primary uveal melanoma cells and metastatic C8161 cutaneous melanoma cells all constricted floating collagen gels in a similar fashion within 48 hours (Figure 5, E and F). In contrast, poorly invasive OCM-1A primary uveal melanoma cells did not constrict the gels at all, and tension lines were not observed anywhere in the gel (Figure 5G), even after 3 weeks. Finally, when the gels were stained with a variety of vital dyes that label mitochondria, we noted that only the aggressive melanoma cell lines formed network patterns as they contracted the gels (Figure 5H).

Next, we tested whether drugs that block the ability of actin microfilaments to transduce forces throughout the cell could block gel contraction reversibly.[24] By targeting actin, we found that the ability of highly invasive and metastatic cells to constrict matrices was blocked with 1 μmol/L cytochalasin-D and that this effect was reversible on removal of the drug (gels were observed to contract after the media was replaced and the drug removed; data not shown). Thus, the biomechanical ability of cells to remodel matrices, a mechanical prerequisite for tube formation, is linked to the invasive and metastatic tumor cell phenotype and does not occur with poorly invasive cells.

Figure 3. Immunohistochemistry of melanoma microcirculation patterns. A: Proliferative diabetic retinopathy, a classic example of an angiogenic response, was used as one control. The discrete vessels stained for Factor VIII-related antigen are not interconnected and do not form loops that encircle domains of tissue in histological section (as shown in Figure 1, A-E and H). B: Higher magnification of proliferative diabetic retinopathy stained for Factor VIII-related antigen. At least five endothelial cell nuclei are identified lining this small vessel. Cells containing brown pigment represent iron in macrophages and reflects vascular incompetence in this neo-angiogenic response. C: Tissue section taken from primary uveal melanoma, stained by PAS without hematoxylin. This patient died of metastatic melanoma. Note the interconnected loops. D: Same tumor as illustrated in C, stained for Factor VIII-related antigen (appears red). The loops stain only focally and discontinuously. E: The same tumor as illustrated in C and D, stained for CD31. Staining of this pattern with CD31 is even less evident than with Factor VIII-related antigen. F: Primary uveal melanoma showing intense CD31 staining (appears red) of tumor cells adjacent to the lumen (*) of intratumoral vascular tube lacking endothelial lining. This patient died of metastasis 6 years after the eye was removed. G: Higher magnification of tumor depicted in D, also stained for Factor VIII-related antigen. Only a segment of this otherwise hollow channel (*) stains for Factor VIII-related antigen. The remainder of the tube is vacant (*). Endothelial cell nuclei are not identified. H: Tissue section stained by Ulex europaeus agglutinin I (appears red) and counterstained with hematoxylin. Endothelial cell nuclei are not identified. Ulex labels the contents of the lumen around the red blood cells. Tumor cells are identified external to the vessel. I: Tissue section stained with CD34 and counterstained with hematoxylin; endothelial cell nuclei are not identified. CD34 labels the lumen contents between the red blood cells. Tumor cells are situated external to the vessel. J: Tissue section stained for KDR (appears red) and counterstained with hematoxylin; endothelial cell nuclei are not identified. The lumen contents are labeled with KDR. Tumor cells are situated external to the vascular channel. K: Tissue section double labeled for CD31 (red chromogen with direct illumination) and L, S-100 protein (same field viewed by reflectance microscopy; immunogold). The vascular channels do not stain for CD31 but cells apposed externally to the vascular channel lumen are positive for S-100 protein, a reaction consistent with melanoma, but not endothelial cells. Tissue stains: A, B, D,F, Factor VIII-related antigen, counterstained with hematoxylin; C, PAS without hematoxylin counterstain; E and G, CD31 counterstained with hematoxylin; H, Ulex europaeus agglutinin I counterstained with hematoxylin; I, CD34, counterstained with hematoxylin; J, KDR, counterstained with hematoxylin; K, CD31 (red chromogen) photographed by direct illumination, L, S-100 protein conjugated to immunogold (same section, same field as K) photographed with epipolarization microscopy. Original magnifications, ×20 (A, C, D, E, K, and L). Scale bar, 25 μm for B,F,G, and H.

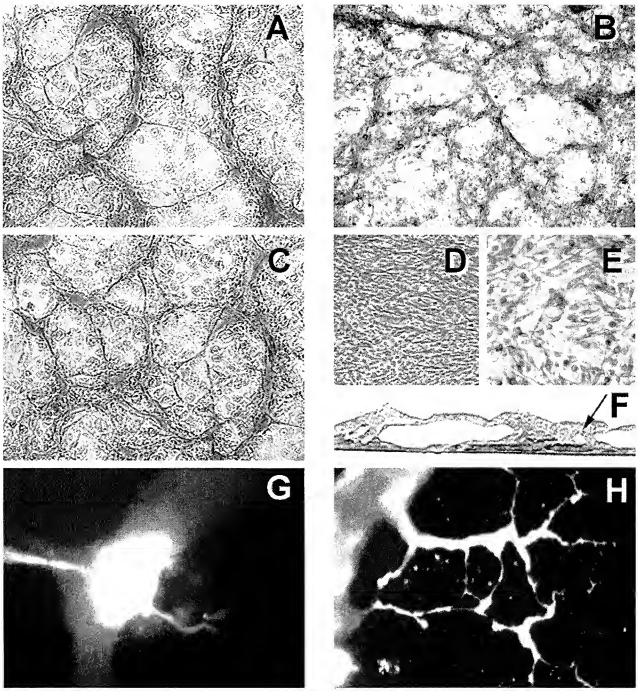

Figure 4. A: PAS-stained phase contrast micrograph of 3D culture of highly invasive M619 human uveal melanoma cells forming patterned networks after 1 week on Matrigel. B: Metastatic uveal melanoma MUM-2B forming patterned networks on dilute Type I collagen (stained with PAS to highlight basement membranes). C: Metastatic cutaneous melanoma C8161 also formed patterned networks after 1 week on Matrigel. By contrast, poorly invasive OCM-1A cells do not form patterned networks on Matrigel (D) or on dilute Type 1 collagen gels (E). F: Histological cross-section of a 2-week, 3D culture of cell line M619 showing both large sinusoidal structures and smaller tubular structures embedded in the monolayer (arrow). G: Fluorescence localization of Texas red dye at the moment of microinjection into a large sinusoid of a mature vessel-forming 3D culture of pure MUM-2B cells. H: The dye distributes through smaller tumor-generated vessels in 30 minutes. Compare with Figure 1G, the confocal angiogram taken of a patient with a uveal melanoma. Original magnifications, ×200 (F); ×40 (all others).

cDNA Microarray Analysis: Comparison between Poorly Invasive and Highly Invasive Melanoma Cells

We compared poorly invasive and highly invasive uveal melanoma cells derived from the same patient using hybridization to cDNA microarrays.[26,43] This approach allowed the expression analysis of 5000 genes simultaneously. Comprehensive results will be provided elsewhere, but, as illustrated in Table 2, numerous genes whose expression patterns were altered in association with the invasive phenotype further validated our histo-

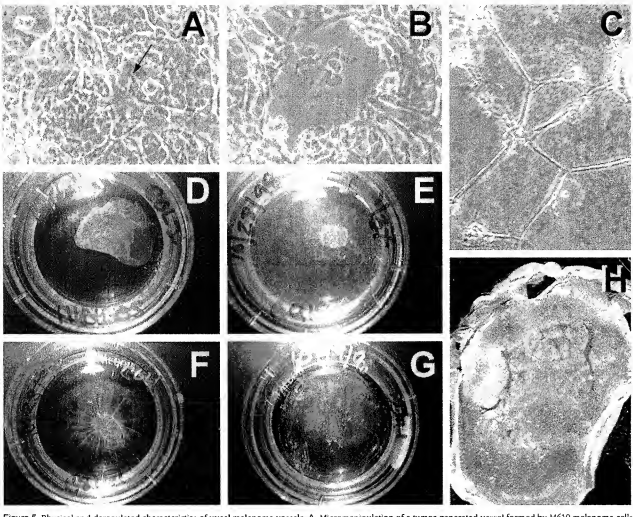

Figure 5. Physical and deregulated characteristics of uveal melanoma vessels. A: Micromanipulation of a tumor-generated vessel formed by M619 melanoma cells and removal of cells (small black arrow) from the acellular vascular channel, and all others. B: subsequent deformation of the same tubular structure for measurement of its mechanical response to applied strain.[24] C: Cord formation by cultured human endothelial cells under identical media and culture conditions shown in A and B. Note that all of the endothelial cells are recruited into tessellations, unlike spheroidal nests of aggressive cultured melanoma cells which are encircled by acellular microvessels of varying diameters (A and B). D–G: Comparison of collagen gel contraction after seeding with HUVECs or tumor cells. Endothelial cells (D) contracted the floating gels in 48 hours, as do aggressive primary C918 intraocular melanoma cells (E) and metastatic C8161 cutaneous melanoma cells (F); however, poorly invasive OCM-1A primary melanoma cells (G) did not contract the floating gels even after 3 weeks' observation. H: Concomitant gel contraction and tube formation on floating hydrated gel. Highly invasive M619 melanoma cells contract the gel and form networks as demonstrated by labeling of tumor cell mitochondria with rhodamine 123.

logical and *in vitro* observations. Briefly summarized, of the 210 known genes that were differentially expressed in these tumor populations, approximately 15 have been associated previously with the endothelial/vascular phenotype. Examples include tyrosine kinase with immunoglobulin and epidermal growth factor homology domains (TIE-1), an endothelial receptor kinase involved in vessel formation and maturation,[44] urokinase-type plasminogen activator (uPA), epithelial cell kinase (ECK),and keratin 8 intermediate filament, which collectively support the deregulated embryonic-like phenotype displayed by the highly invasive melanoma cells.[45] A series of genes that would generate relevant biological molecules to form microvascular channels were also observed to be overexpressed in the aggressive melanoma cells including connective tissue growth factor (CTGF), the extracellular matrix-associated fibrillin, collagens VI[17] and I, and fibronectin. Genes shown to be underexpressed in the highly invasive cells included myosin light-chain kinase, whose deregulation product might alter actomyosin interactions. In summary, the cDNA microarray analysis of highly invasive *versus* poorly invasive melanoma tumor cells confirmed a genetic reversion to a pluripotent embryonic-like genotype in the highly aggressive melanoma cells.

Discussion

Until now, it has been taken for granted that all intratumoral vascular channels are formed and lined by endothelial cells. The demonstration that human melanoma cells containing melanosomes and premelanosomes are found lining patterned vascular channels in patients' pri-

Table 2. Microarray Analysis of Highly Invasive/Metastatic *versus* Poorly Invasive Uveal Melanoma Cells

Protein	Symbol	Unigene	Function	Ratio*
Endothelial receptor kinase	TIE-1	Hs.78824	Receptor tyrosine kinase	>100
Urokinase-type plasminogen activator	PLAU	Hs.77274	Proteolysis	80
Epithelial cell kinase	ECK	Hs.32197	Receptor tyrosine kinase	77
Connective tissue growth factor	CTGF	Hs.75511	Growth factor	35
Keratin 8	KRT8	Hs.78271	Intermediate filament	18
Fibrillin	FNB1	Hs.750	Extracellular matrix	12
Collagen VI	COL6A1	Hs.80988	Extracellular matrix	6.7
Fibronectin	FN1	Hs.100056	Extracellular matrix	4.2
Collagen I, α-2	COL1A2	Hs.90283	Extracellular matrix	2.5
Myosin light chain kinase	MYLK	Hs.75950	Regulator of contractility	0.12

Altered gene expression in human uveal melanoma cells was identified by cDNA microarray analysis.
*Relevant expression of selected genes significant for vascular channel formation is reported as the ratio of highly invasive and metastatic to poorly invasive uveal melanoma cells.

mary and metastatic tumors, and that these tumor cells generate a functional perfusable network *in vitro*, calls for reappraisal of the current assumption that endothelial cell-mediated angiogenesis is the only mechanism underlying or responsible for tumor growth and metastasis.

Our observations address the intriguing cellular and molecular mechanisms underlying the formation of patterned vascular channels found in the most aggressive primary intraocular (uveal) melanomas and their metastases and in metastatic cutaneous melanomas. The data reveal that: (i) the patterned vascular channels of aggressive primary and metastatic melanoma are different from endothelial-derived angiogenic vessels; (ii) highly invasive melanoma cells, but not poorly invasive ones, reconstitute the patterned vascular channels seen in human tumor tissue *in vitro* in the absence of endothelium; (iii) the tumor cells that generate the patterned vascular channels are deregulated and aberrantly express genes heretofore associated with embryonic stem cells including those associated with primordial vascular development; and (iv) the generation of patterned vascular channels by deregulated aggressive tumor cells in human melanomas is a novel pathway to generate microcirculation in a tumor and facilitate metastasis.

The patterned vascular channels characteristic of aggressive primary and metastatic melanoma are different from angiogenic vessels in that (i) vascular channels in aggressive melanomas are embedded in highly patterned matrix (Figure 1, B-D), whereas angiogenic vessels (the growth of new blood vessels from a pre-existing microcirculation) are characterized by clusters of vessels and are not patterned (Figure 3, A and B); (ii) the patterned melanoma vascular channels were not found to be lined by endothelium by light microscopy (Figures 1E, 2B, and 3, F-L), transmission electron microscopy (Figure 2, B and C), and immunohistochemistry (Figure 3, D-L), whereas the contribution of an endothelium to angiogenic vessels in proliferative diabetic retinopathy and normal vessels in the adjacent normal tissue is clearly identified by light microscopy and immunohistochemistry (Figure 3, A and B); and (iii) the architecture of the matrix-associated vascular channels, characterized by interconnected loops and networks, although not typical of angiogenesis, is characteristic of vasculogenesis (formation of networked microvasculature by incorporation of cells).[2]

Highly invasive melanoma cells reconstitute *in vitro* the patterned matrix-associated vascular channels seen in human melanomas in the absence of endothelial cells and fibroblasts. In contrast, poorly invasive melanoma cells are not capable of generating the biomechanical properties (ie, capable of contracting matrices) required to generate patterned acellular vascular channels *in vitro*. The ability of highly invasive, but not poorly invasive, melanoma cells to generate patterned vascular channels *in vitro* helps to explain the very strong association between the presence of the vascular channel-associated patterns in patient tissues and death from metastatic melanoma (Figure 1F).[4]

The formation of a microcirculation by cells other than endothelial cells has been reported in normal embryonic tissues, but not previously in the context of tumor progression. For example, there is strong evidence suggesting that human cytotrophoblasts adopt an endothelial cell phenotype as they participate in the establishment of the human placenta and primordial microcirculation.[46–48] Indeed, invasive melanoma cells capable of generating a patterned microcirculation *in vitro* express inappropriate markers. For example, we previously showed that highly invasive and metastatic melanoma cells (but not poorly invasive cells) express embryonic keratins in addition to their classical vimentin intermediate filament marker.[45] Moreover, highly invasive, but not poorly invasive, melanoma cells express the *c-met* proto-oncogene and demonstrate responsiveness to scatter factor (HGF/SF), a potent mitogen, morphogen, and motogen.[49] Finally, cDNA microarray analysis, comparing poorly invasive with highly invasive melanoma cells, discloses a variety of differential gene expression associated with a combination of phenotypes including endothelium (TIE-1) and epithelium (keratin 8), suggesting a genetic reversion to a pluripotent embryonic-like phenotype. The ability of highly invasive melanoma cells to generate patterned vascular channels may be one of many important pluripotent manifestations of this embryonic-like phenotype, which ensures remodeling, perfusion, tumor cell viability, and a dissemination mechanism.

Analysis of differential gene expression between highly and poorly invasive melanoma cells supports our observation that highly invasive cells generate a patterned paracirculation *in vitro*. The underexpression of myosin

light chain kinase,[50] a regulator of contractility, in highly invasive melanoma cells is consistent with the differential ability of these, but not of poorly invasive melanoma cells, to contract matrices and form a patterned paracirculation (Figures 4 and 5).

Our data suggest that tumor cell-generated vascular channels provide a blood supply required for growth and metastasis without the influence of soluble tropic factors associated with stimulated angiogenesis in other contexts, such as diabetic retinopathy in the eye. The generation of highly patterned and functional vascular channels by the tumor itself is a marker of the aggressive tumor cell phenotype. The generation of the patterned melanoma microcirculation is vasculogenic mimicry mediated by the tumor cells themselves and may function independently of tumor angiogenic mechanisms during various phases of tumor progression. Therefore, the unique observations reported here should serve as a catalyst for exploring patterned vascular channel formation in other tumors and may provide new clues for the development of novel treatment modalities that target the molecular basis for the unique architecture of the tumor-generated microcirculation.[51,52]

Acknowledgments

We gratefully acknowledge the participation of Drs. Karla J. Daniels and H. Culver Boldt in the generation of some of the uveal melanoma cell lines used in this study. Cell line OCM-1A was a gift from Dr. June Kan-Mitchell. Drs. R. Jean Campbell and Mary G. Mehaffey contributed clinical material to these studies, and Drs. William Freeman and Arthur Mueller collaborated in studying patients angiographically. We also thank Peggy Meyer for specialized image processing. We are especially grateful to Dr. Erkki Ruoslahti for his critical scientific input and editing of the manuscript, and to Drs. Judah Folkman, Donald Ingber, Robert Kerbel, and Isaiah Fidler for their insightful comments. We appreciate the helpful scientific discussions provided by Dr. Richard Seftor.

References

1. Folkman J: Clinical applications of research on angiogenesis. Seminars in Medicine of the Beth Israel Hospital, Boston. New Engl J Med 1995, 333:1757–1763
2. Risau W: Mechanisms of angiogenesis. Nature 1997, 386:671–674
3. Weidner N: Tumoral vascularity as a prognostic factor in cancer patients: the evidence continues to grow. J Pathol 1998, 184:119–122
4. Folberg R, Rummelt V, Parys-Van Ginderdeuren R, Hwang T, Woolson RF, Pe'er J, Gruman LM: The prognostic value of tumor blood vessel morphology in primary uveal melanoma. Ophthalmology 1993, 100:1389–1398
5. McLean IW, Foster WD, Zimmerman LE, Gamel JW: Modifications of Callender's classification of uveal melanoma at the Armed Forces Institute of Pathology. Am J Ophthalmol 1983, 96:502–509
6. Folberg R, Mehaffey M, Gardner LM, Meyer M, Rummelt V, Pe'er J: The microcirculation of choroidal and ciliary body melanomas. Eye 1997, 11:227–238
7. Folberg R, Pe'er J, Gruman LM, Woolson RF, Jeng G, Montague PR, Moninger TO, Yi H, Moore KC: The morphologic characteristics of tumor blood vessels as a marker of tumor progression in primary human uveal melanoma: a matched case-control study. Hum Pathol 1992, 23:1298–1305
8. McLean IW, Keefe KS, Burnier MN: Uveal melanoma: comparison of the prognostic value of fibrovascular loops, mean of the ten largest nucleoli, cell type and tumor size. Ophthalmology 1997, 104:777–780
9. Pe'er J, Rummelt V, Maswi L, Hwang T, Woolson RF, Folberg R: Mean of the ten largest nucleoli, microcirculation architecture, and prognosis of ciliochoroidal melanomas. Ophthalmology 1994, 101:1227–1235
10. Mehaffey MG, Folberg R, Meyer M, Bentler SE, Hwang T, Woolson RF, Moore KC: Relative importance of quantifying area and vascular patterns in uveal melanoma. Am J Ophthalmol 1997, 123:798–809
11. Bartsch D-U, Weinreb RN, Zinser G, Freeman WR: Confocal scanning infrared laser ophthalmoscopy for indocyanine green angiography. Am J Ophthalmol 1995, 120:642–651
12. Schneider U, Gelisken F, Inhoffen W, Kreissig I: Indocyanine-green videoangiography of malignant melanomas of the choroid using the scanning laser ophthalmoscope. Ger J Ophthalmol 1996, 5:6–11
13. Mueller AJ, Bartsch DU, Folberg R, Mehaffey MG, Boldt HC, Meyer M, Gardner LM, Goldbaum MH, Peer J, Freeman WR: Imaging the microvasculature of choroidal melanomas with confocal indocyanine green scanning laser ophthalmoscopy. Arch Ophthalmol 1998, 116:31–39
14. Folberg R, Verdick RE, Weingeist TA, Montague PR: Gross examination of eyes removed for ciliary body or choroidal melanoma. Ophthalmology 1986, 93:1643–1647
15. Hendrix MJ, Seftor EA, Seftor RE, Trevor KT: Experimental co-expression of vimentin and keratin intermediate filaments in human breast cancer cells results in phenotypic interconversion and increased invasive behavior. Am J Pathol 1997, 150:483–495
16. Rummelt V, Mehaffey MG, Campbell RJ, Peer J, Bentler SE, Woolson RF, Naumann GOH, Folberg R: Microcirculation architecture of metastases from primary ciliary body and choroidal melanomas. Am J Ophthalmol 1998, 126:303–305
17. Daniels KJ, Boldt HC, Martin JA, Gardner LM, Meyer M, Folberg R: Expression of Type VI collagen in uveal melanoma: role in pattern formation and tumor progression. Lab Invest 1996, 75:55–66
18. Welch DR, Bisi JE, Miller BE, Conaway D, Seftor EA, Yohem KH, Gilmore LB, Seftor RE, Nakajima M, Hendrix MJ: Characterization of a highly invasive and spontaneously metastatic human malignant melanoma cell line. Int J Cancer 1991, 47:227–237
19. Stamer WD, Huang Y, Seftor RE, Svensson SS, Snyder RW, Regan JW: Cultured human trabecular meshwork cells express functional α 2A adrenergic receptors. Invest Ophthalmol Vis Sci 1996, 37:2426–2433
20. Seftor EA, Seftor REB, Way DL, Bernas M, Weinland CL, Witte CL, Witte MH, Hendrix MJC: Enhancement of endothelial cell and Kaposi sarcoma migration by selective chemoattractants. Lymphol 1994, 27:755–758 (suppl)
21. Xu Y, Swerlick RA, Sepp N, Bosse D, Ades EW, Lawley TJ: Characterization of expression and modulation of cell adhesion molecules on an immortalized human dermal microvascular endothelial cell line (HMEC-1). J Invest Dermatol 1994, 102:833–837
22. Hendrix MJ, Seftor EA, Seftor RE, Fidler IJ: A simple quantitative assay for studying the invasive potential of high and low human metastatic variants. Cancer Lett 1987, 38:137–147
23. Hendrix MJC, Seftor EA, Chu YW, Trevor KT, Seftor REB: Role of intermediate filaments in migration, invasion and metastasis. Cancer Metastasis Rev 1996, 15:507–525
24. Maniotis A, Chen C, Ingber D: Demonstration of mechanical interconnections between integrins, cytoskeletal filaments, and nuclear scaffolds that stabilize nuclear structure. Proc Natl Acad Sci USA 1997, 94:849–854
25. Eckes B, Dogic D, Colucci-Guyon E, Wang N, Maniotis A, Ingber D, Merckling A, Langa F, Aumailley M, Delouvee A, Koteliansky V, Babinet C, Krieg T: Impaired mechanical stability, migration and contractile capacity in vimentin-deficient fibroblasts. J Cell Sci 1997, 94:1897–1907
26. DeRisi J, Penland L, Brown PO, Bittner ML, Meltzer PS, Ray M, Chen Y, Su YA, Trent JM: Use of a cDNA microarray to analyse gene expression patterns in human cancer [see comments]. Nat Genet 1996, 14:457–460
27. Khan J, Simon R, Bittner M, Chen Y, Leighton SB, Pohida T, Smith PD, Jiang Y, Gooden GC, Trent JM, Meltzer PS: Gene expression profiling

of alveolar rhabdomyosarcoma with cDNA microarrays. Cancer Res 1998, 58:5009–5013
28. Schuler GD, Boguski MS, Stewart EA, Stein LD, Gyapay G, Rice K, White RE, Rodriguez-Tome P, Aggarwal A, Bajorek E, Bentolila S, Birren BB, Butler A, Castle AB, Chiannilkulchai N, Chu A, Clee C, Cowles S, Day PJ, Dibling T, Drouot N, Dunham I, Duprat S, East C, Hudson TJ: A gene map of the human genome. Science 1996, 274:540–546
29. McLean IW: The biology of haematogenous metastasis in human uveal malignant melanoma. Virchows Arch A Pathol Anat 1993, 422: 433–437
30. Sakamoto T, Sakamoto M, Yoshikawa H, Hata Y, Ishibashi T, Ohnishi Y, Inomata H: Histologic findings and prognosis of uveal malignant melanoma in Japanese patients. Am J Ophthalmol 1996, 121:276–283
31. Makitie T, Summanen P, Tarkannen A, Kivela T: Microvascular loops and networks as prognostic indicators in choroidal and ciliary body melanomas. J Natl Cancer Inst 1999, 91:359–367
32. Rummelt V, Folberg R, Rummelt C, Gruman LM, Hwang T, Woolson RF, Yi H, Naumann GOH: Microcirculation architecture of melanocytic nevi and malignant melanomas of the ciliary body and choroid. A comparative histopathologic and ultrastructural study. Ophthalmology 1994, 101:718–727
33. Folberg R, Fleck M, Mehaffey MG, Meyer M, Bentler SE, Woolson RF, Pe'er J: Mapping prognostically significant vascular patterns in ciliary body and choroidal melanomas. Pathol Oncol Res 1996, 2:229–236
34. Mehaffey MG, Gardner LM, Folberg R: Distribution of prognostically important vascular patterns across multiple levels in ciliary body and choroidal melanomas. Am J Ophthalmol 1998, 126:373–378
35. Rummelt V, Gardner LM, Folberg R, Beck S, Knosp B, Moninger TO, Moore KC: Three-dimensional relationships between tumor cells and microcirculation using double cyanine-immunolabeling, laser scanning confocal microscopy and computer-assisted reconstruction: an alternative to cast corrosion preparations. J Histochem Cytochem 1994, 42:681–686
36. Silverman RH, Folberg R, Boldt HC, Rondeau MJ, Lloyd HO, Mehaffey MG, Lizzi FL, Coleman DJ: Correlation of ultrasound parameter imaging with microcirculatory patterns in uveal melanomas. Ultrasound Med Biol 1997, 23:573–581
37. Folkman J, Haudenschild C: Angiogenesis in vitro. Nature 1980, 288:551–556
38. Ingber DE, Folkman J: Mechanochemical switching between growth and differentiation during fibroblast growth factor-stimulated angiogenesis in vitro: role of extracellular matrix. J Cell Biol 1989, 198:317–330
39. Nicosia RF, Ottinetti A: Modulation of microvascular growth and morphogenesis by reconstituted basement membrane gel in three-dimensional cultures of rat aorta: a comparative study of angiogenesis in matrigel, collagen, fibrin, and plasma clot. In Vitro Cell Dev Biol 1990, 26:119–128
40. Vernon RB, Sage EH: Between molecules and morphology extracellular matrix and creation of vascular form. Am J Pathol 1995, 147 873–883
41. Vernon RB, Lara SL, Drake CJ, Iruelaarispe ML, Angello JC, Little CD, Wight TN, Sage EH: Organized type I collagen influences endothelial patterns during spontaneous angiogenesis in vitro: planar cultures as models of vascular development. In Vitro Cell Dev Biol Anim 1995, 31:120–131
42. Klein CE, Dressel D, Steinmayer T, Mauch C, Eckes B, Krieg T, Bankert RB, Weber L: Integrin $\alpha 2\beta 1$ is upregulated in fibroblasts, and highly aggressive melanoma cells in three-dimensional collagen lattices, and mediates the reorganization of collagen I fibrils. J Cell Biol 1991, 115:1427–1436
43. Khan J, Simon R, Bittner M, Chen Y, Leighton SB, Pohieda T, Smith P, Jiang U, Gooden JC, Trent JM, Meltzer PS: Gene expression profiling of alveolar rhabdomyosarcoma with cDNA microarrays. Cancer Res 1998, 58:5009–5013
44. McCarthy MJ, Crowther M, Bell PR, Brindle NP: The endothelial receptor tyrosine kinase tie-1 is upregulated by hypoxia and vascular endothelial growth factor. FEBS Lett 1998, 423:334–338
45. Hendrix MJC, Seftor EA, Seftor RB, Gardner LM, Boldt HC, Meyer M, Peer J, Folberg R: Biologic determinants of uveal melanoma metastatic phenotype - role of intermediate filaments as predictive markers. Lab Invest 1998, 78:153–163
46. Zhou Y, Damsky CH, Fisher SJ: Preeclampsia is associated with failure of human cytotrophoblasts to mimic a vascular adhesion phenotype: one cause of defective endovascular invasion in this syndrome? J Clin Invest 1997, 99:2152–2164
47. Zhou Y, Fisher SJ, Janatpour M, Genbacev O, Dejana E, Wheelock M, Damsky CH: Human cytotrophoblasts adopt a vascular phenotype as they differentiate: a strategy for successful endovascular invasion? J Clin Invest 1997, 99:2139–2151
48. Damsky CH, Fisher SJ: Trophoblast pseudo-vasculogenesis: faking it with endothelial adhesion receptors. Curr Opin Cell Biol 1998, 10: 660–666
49. Hendrix MJC, Seftor EA, Seftor REB, Gardner LM, Boldt HC, Meyer M, Pe'er J, Folberg R: Regulation of uveal melanoma interconverted phenotype by hepatocyte growth factor/scatter factor (HGF/SF). Am J Pathol 1998, 152:855–863
50. Fujita K, Ye LH, Sato M, Okagaki T, Nagamachi Y, Kohama K: Myosin light chain kinase from skeletal muscle regulates an ATP-dependent interaction between actin and myosin by binding to actin. Mol Cell Biochem 1999, 190:85–90
51. Ruoslahti E, Engvall E: Integrins and vascular extracellular matrix assembly. J Clin Invest 1997, 100:S53–S56
52. Arap W, Pasqualini R, Ruoslahti E: Cancer treatment by targeted drug delivery to tumor vasculature in a mouse model. Science 1998, 279: 377–380

American Journal of Pathology, Vol. 151, No. 5, November 1997

Non-Small-Cell Lung Carcinoma Tumor Growth without Morphological Evidence of Neo-Angiogenesis

Francesco Pezzella,* Ugo Pastorino,† Elda Tagliabue,‡ Salvatore Andreola,§ Gabriella Sozzi,‖ Giampietro Gasparini,¶ Sylvie Menard,‡ Kevin C. Gatter,# Adrian L. Harris,** Steve Fox,# Marc Buyse,†† Silvana Pilotti,§ Marco Pierotti,‖ and Franco Rilke§

From the Department of Histopathology, University College London, and the Department of Thoracic Surgery,† Royal Brompton Hospital, London, and the Department of Cellular Science# and ICRF Clinical Oncology Unit,** University of Oxford, Oxford, United Kingdom; the Division of Pathology,‡ Experimental Oncology E§ and A,‖ Istituto Nazionale Tumori, Milano, and the Department of Oncology,¶ St. Bortolo Hospital, Vicenza, Italy; and the Institute for Drug Development-ID2,†† Brussels, Belgium*

Neoplastic growth is usually dependent on blood supply, and it is commonly accepted that this is provided by the formation of new vessels. However, tumors may be able to grow without neovascularization if they find a suitable vascular bed available. We have investigated the pattern of vascularization in a series of 500 primary stage I non-small-cell lung carcinomas. Immunostaining of endothelial cells has highlighted four distinct patterns of vascularization. Three patterns (which we called basal, papillary, and diffuse) have in common the destruction of normal lung and the production of newly formed vessels and stroma. The fourth pattern, which we called alveolar or putative nonangiogenic, was observed in 16% (80/500) of the cases and is characterized by lack of parenchymal destruction and absence of both tumor-associated stroma and new vessels. The only vessels present were the ones in the alveolar septa, and their presence highlighted, through the whole tumor, the lung alveoli filled up by the neoplastic cells. This observation suggests that, if an appropriate vascular bed is available, a tumor can exploit it and grows without inducing neo-angiogenesis. This could have implications for strategies aimed at inhibiting tumor growth by vascular targeting or inhibition of angiogenesis. ***(Am J Pathol 1997, 151:1417–1423)***

In recent years, the essential role played by angiogenesis in neoplastic growth has been carefully investigated. The hypothesis that tumor growth is dependent on angiogenesis was formulated in 1971 by Folkman[1] who later stated it in the following terms: "Once a tumor 'take' has occurred, every increase in tumor cell population must be preceded by an increase in new capillaries converging on the tumor."[2]

A large number of studies have demonstrated that tumors grow first with-an avascular phase in which they do not became larger than 1 or 2 mm, and any further growth must be supported by growth of new vessels.[2] Tumor angiogenesis (ie, growth of new vessels) is not an isolated phenomenon but is part of a complex process that involves destruction of the existing normal parenchyma by enzymes such as metalloproteinases and remodeling of extracellular matrix surrounding the vessels from which buds of new vessels emerge. Production of newly formed extracellular matrix, the so-called tumor-associated stroma, must occur as well to support both the new vessels and the neoplastic cells.[3–5] To trigger this series of events, essential for successful growth, the tumor cells must be able to produce a variety of enzymes, growth factors, and angiogenic factors as well as inhibiting the synthesis of other molecules that posses anti-angiogenic activity.[4]

The clinical relevance of intratumor microvessel density has been highlighted by studies demonstrating, in a variety of different malignancies, that the higher the microvessel density, the poorer the clinical outcome.[6–9] In all of these studies, tumor vascularization has always been considered as synonymous with neo-anglogenesis. This assumption is based on the fact that the normal tissue has been replaced by the neoplasm and that new vessels have developed within the tumor-associated stroma. This leads to the conclusion that, to grow, a tumor needs to produce new vessels and that the richer this vascularization, the better the growth.

Another hypothesis is that, if a tumor can obtain an efficient blood supply from a suitable vascular bed that already exists, then it could grow without the production of new vessels. The association between high microvessel density and poor prognosis has not been demon-

Supported by three grants from Associazione Italiana per la Ricerca sul Cancro (to F. Pezzella, G. Gasparini, and U. Pastorino)

Accepted for publication July 23, 1997.

Address reprint requests to Dr. Francesco Pezzella, Department of Histopathology, University College London, Rockfeller Building, University Street, London, WC1E 6JJ, UK.

Table 1. Characteristics of the 500 Stage I Patients Undergoing Resection for Non-Small-Cell Carcinoma of the Lung Investigated in the Present Study

	Number of patients (%)	Sex (M/F)	Smokers	Mean cigarettes per day	Nonsmokers	Not known	T stage	
							T1	T2
Adenocarcinoma	210 (42%)	191/19	188	26.8	17 (8.3%)	5	66 (31.5%)	144 (68.5%)
Squamous carcinoma	245 (49%)	236/9	236	26.2	2 (0.9%)	7	57 (23.3%)	188 (76.7%)
Others*	45 (9%)	39/6	39	29.9	6 (13%)		5 (11%)	40 (89%)
All types	500	466/34	463 (94.9%)	26.6	25 (5.5%)	12	128 (25.6%)	372 (74.4%)

*Eleven bronchioalveolar, fifteen large-cell, three adenosquamous, and sixteen mucoepidermoid.

strated in all tumors. In squamous cell carcinoma of the tongue,[10] no association has been found with overall survival and node metastases. The above hypothesis could explain these contradictory findings; if, in highly vascularized organs, such as the tongue, the pre-existing vessels were able to provide the blood supply essential for tumor progression, they, rather than the intratumor newly formed vessels, could dictate the clinical course of the tumor.[7]

Studies of non-small-cell carcinoma of the lung have shown that intratumor microvessel density is relevant to progression and is associated with lymph node node status.[11–17] We have recently investigated[18] the prognostic value of a group of biological markers in a large series of primary stage I (pT1 pT2 N0) non-small-cell carcinomas of the lung undergoing surgery, and among the markers analyzed were the intratumor vessels. It was noticed that in a subgroup of non-small-cell carcinoma there was no evidence of neo-angiogenesis, but the tumor appeared to exploit the existing lung vessels.

The aim of the present study is to describe in detail the histological features of the vascular patterns in these tumors and their correlation with some clinical and biological characteristics.

Materials and Methods

Clinical Details

From January 1974 to December 1990, 608 consecutive patients underwent surgical resection at the Division of Thoracic Surgery of the Istituto Nazionale Tumori (Milano, Italy) for pathological stage I (pT1–2, N0, M0, R0)[19] non-small-cell lung cancer. After pathological review and immunostaining for CD31, 500 patients were included in the present study. The main clinical features of these patients are illustrated in Table 1. Clinical follow-up was intensive in this population with the purpose of detecting relapse and second primary tumors and consisted of routine sputum cytology and chest x-rays every 3 months during the first 3 years, every 6 months up to 5 years, and yearly thereafter. The follow-up was updated in July 1995, with a median time of observation of 64 months overall and 102 months for alive patients.

Pathological Classification

All of the histopathological specimens (formalin fixed and paraffin embedded) available for each patient were retrieved from the files of the Division of Pathology of the Istituto Nazionale Tumori and reviewed to select the most suitable samples for analysis. At least one representative sample for each tumor was selected. The histopathological typing was performed on conventional hematoxylin and eosin staining according to the World Health Organization[20] and the Armed Forces Institute of Pathology.[21] In mixed types, the distinction between squamous carcinomas and adenocarcinomas was made according to the predominant cell type. In addition to histopathological classification, these sections were used for immunocytochemical analysis.

Immunocytochemistry

Blood vessels were identified by immunostaining with the anti-CD31 JC70 monoclonal antibody[22] (courtesy of Dr. D. Mason, Oxford). The following immunocytochemical markers were also tested: the laminin receptor (Ab M-Luc5),[23] associated with invasion and metastases; the proto-oncogene products of C-*erb*B1/*EGFR* (Ab 31G7, TRITON Diagnostic, Alameda, CA) and *bcl-2*[24] (clone 100, courtesy of Dr. D. Mason,

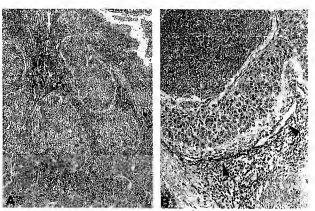

Figure 1. Basal pattern, immunostaining for CD31 (antibody JC70; immunoperoxidase/AEC method). A: Nests of neoplastic epithelial cells are surrounded by stroma in which vessels are present. Magnification, ×25. B: Vessels are present in the stroma beneath the neoplastic epithelium (arrows). Magnification, ×100.

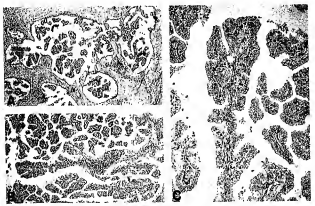

Figure 2. Papillary pattern, immunostaining for CD31 (antibody JC70; immunoperoxidase/AEC method). A and B: Tumor with papillary pattern surrounded by tumor-associated stroma. Magnification, ×25 (A) and ×40 (B). C: Papillae made up by a fibrous stalk lined by neoplastic cells. Immunostaining for CD31 shows vessels in the stalk. Magnification, ×100.

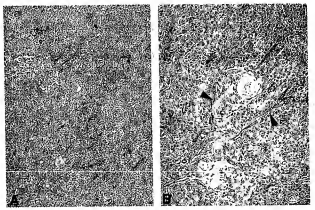

Figure 3. Diffuse pattern, immunostaining for CD31 (antibody JC70; immunoperoxidase/AEC method). A: A diffuse neoplastic proliferation without any identifiable architecture is seen. Magnification, ×25. B: Vessels and stroma (**arrows**) are randomly scattered throughout the tumor, mixed up with the neoplastic epithelial cells. Magnification, ×100.

Oxford); and the tumor suppressor gene product p53 (Ab DO7, Ylem-Novocastra, Newcastle upon Tyne, UK).

Briefly, formalin-fixed, paraffin-embedded tissue sections were cut and mounted on slides coated with poly-L-lysine (Sigma Chemical Co., St. Louis, MO), dewaxed in xylene, and rehydrated in alcohol, and endogenous peroxidase activity was blocked by treatment for 30 minutes with 3% hydrogen peroxide in methanol. Each antibody immunodetection was investigated using biotinylated goat anti-mouse or -rabbit IgG (Dako, Carpinteria, CA) followed by a final incubation with steptavidin-conjugated horseradish peroxidase (Dako). The peroxidase activity was detected by aminoethyl carbazole (AEC). For p53, Bcl-2, and CD31 staining, before inactivation of endogenous peroxidase activity, the sections were immersed in 10 mmol/L citrate buffer (in distilled water, pH 6.0) and subjected to microwave irradiation for two cycles of 8 and 5 minutes, separated by a 5-minute pause at 700 W.[25] For epidermal growth factor receptor (EGFR) immunostaining, before treatment with the primary antibody, sections were subjected to enzyme digestion for 5 minutes at 37°C with 0.1% Pronase E (Sigma). Staining without antibody was routinely performed as a negative control procedure.

Evaluation of Tumor Vascularity

Microvessel density was evaluated by the use of the Chalkley grid.[26] Briefly, vessel counting was performed in three areas of maximal vascularization where the highest number of discrete microvessels was stained. Vessel count was then estimated using a 25-point Chalkley eyepiece grid at ×200 magnification. The grid was rotated in the eyepiece to where the maximal number of grid dots overlay immunohistochemically identified vessels or their lumina.

Statistical Analysis

The 2×2 and $r \times c$ frequency tables, the two-sample *t*-test, and the value of *F* with the one-way analysis of variance were calculated as described by Altman.[27]

Results

Description of Vascular Architecture in Non-Small-Cell Lung Carcinomas

Immunostaining of endothelial cells in these 500 cases has highlighted four distinct patterns of vascularization in lung tumors.

Basal

The basic structure of a mucosa is reproduced. Neoplastic cells are arranged in epithelial nests surrounded by connective tissue. Most of the vessels are in the connective tissue beneath the neoplastic epithelium (Figure 1).

Papillary

In this pattern, the vessels are in a stromal stalk, which is covered by neoplastic cells, mostly as a monolayer (Figure 2). The normal lung alveolar pattern is usually recognizable in some areas of the tumor, but remodeling of the alveolar structure with destruction of normal lung and papillary growth invariably occurs (Figure 2).

Diffuse

The normal lung architecture is diffusely replaced. New vessels and stroma are produced intimately admixed with neoplastic cells but without any recognizable architectural structure (Figure 3).

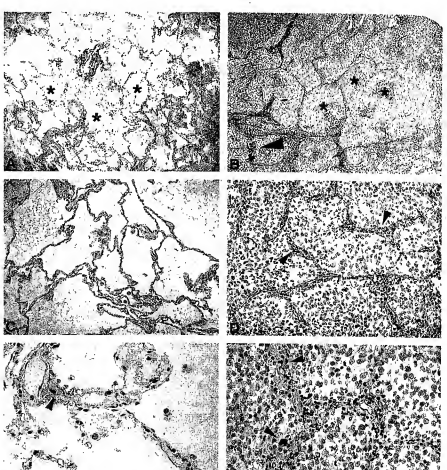

Figure 4. Alveolar pattern, immunostaining for CD31 (antibody JC70; immunoperoxidase/AEC method). A: Normal lung in which air-filled alveolar spaces are identified by asterisks. Magnification, ×25. B: Lung in which a carcinoma is growing with an alveolar pattern; staining for CD31 shows the alveolar vessels highlighting the normal lung architecture. This pattern is present throughout the whole lesion. The alveolar spaces (asterisks) are now filled up by neoplastic epithelial cells. Some anthracytic pigment is present in the trapped parenchyma (arrow). Magnification, ×40. C: Normal lung. Magnification, ×100. D: Alveolar spaces filled up by tumor cells. The only visible vessels (arrows) are in the trapped alveolar septum. Magnification, ×100. E: Normal lung. Anthracytic pigment is present in the alveolar septa (arrows). Magnification, ×160. F: Anthracytic pigment can be seen in the trapped alveolar septum (arrows). Magnification, ×160.

Alveolar

The only vessels evident in this pattern arises from the alveolar septa and highlight the alveolar network of the lung entrapped by neoplastic cells (Figure 4). The likelihood that the vessels observed are the alveolar vessels is suggested not only by their arrangement according to the normal lung architecture but also by the presence in the surrounding stroma tissue of anthracytic pigment (Figure 4, B, E, and F). The amount of anthracytic pigment is highly variable from case to case but within the same lung appears to be comparable inside the tumor and in the surrounding uninvolved parenchyma. The tumor grows in a solid fashion filling the alveolar spaces. Neither endothelial cells nor tumor-associated stroma are present among the neoplastic cells. An alveolar pattern of spread is very common, also in this series, at the periphery of lung tumors[21,28]; we have classified as alveolar (nonangiogenic) cases only the ones presenting this pattern through the whole tumor and not just on the edge.

The first three patterns have in common the destruction of normal lung and production of newly formed vessels and stroma. The alveolar pattern is characterized by lack of parenchyma destruction, lack of tumor-associated stroma, and lack of intratumor vessels; we have therefore considered cases with this pattern as putative nonangiogenic tumors.

We have classified our series of tumors according to these patterns. When more than one pattern was present it was scored according the predominant one, as for standard lung cancer grading.[29] The alveolar pattern accounted for 16% (Table 2) of the cases. In 34 of 80 cases classified as alveolar, a second pattern was present, but it never accounted for more than 5% of the tumor.

Association with Clinico-Pathological Factors

No differences were found, using the two-sample *t*-test, when comparing patients with angiogenic *versus* patients with putative nonangiogenic tumors for sex, age, or mean of daily cigarettes smoked and smoking status (data not shown). However, when the four patterns were compared separately using the $r \times c$ frequency tables as shown in Table 2, the incidence of nonsmokers was lower than expected among patients with basal pattern and higher among patients with papillary pattern. An uneven incidence of female patients was observed among the four groups; it was lower than expected among patients with

basal pattern and higher among patients with papillary pattern (Table 2).

The average microvessel density in angiogenic and putative nonangiogenic tumors is the same (by the one-way analysis of variance); however, it must be kept in mind that the vessels counted in the putative nonangiogenic tumors are the normal lung vessels trapped by the tumor. No difference was found as far as the stage of the tumor was concerned by performing an analysis with frequency tables. Using the same technique, a significant association was found between vascular patterns and histiotype ($P < 0.0005$; Table 2); the basal pattern was associated with squamous cell carcinomas and the papillary with adenocarcinomas whereas the diffuse and the alveolar patterns were equally represented in both. Also, the grading was significantly associated with patterns ($P < 0.0005$; Table 2); the papillary pattern was associated with well differentiated whereas the diffuse and alveolar patterns were present in poorly differentiated carcinomas.

The relationship between the vascular patterns and the biological markers has been investigated by the $r \times c$ frequency tables and is detailed in Table 3. An association has been found between all of the four markers investigated and the vascular patterns. The basal pattern had a higher incidence than expected of cases expressing *bcl-2* and laminin receptor, and the papillary pattern showed a lower number of Bcl-2, p53, and EGFR-positive tumors. A lower incidence of Bcl-2-positive and laminin-receptor-positive cases characterized the diffuse pattern whereas the alveolar had a higher incidence of tumors expressing *bcl-2*.

In Table 2 we show that an association is also present between the alveolar pattern and a higher incidence of distant metastases ($P < 0.025$, as calculated by 2×2 frequency tables). When we looked at the site of metastases, a higher incidence of bone, nodal, and brain recurrence in patients with alveolar tumors is seen, although statistical significance is not reached.

A summary of the main characteristics of the four types of tumors identified is reported in Table 4.

Discussion

In this paper we report a novel finding: the identification of clinically detectable carcinomas that have no morphological evidence of neo-angiogenesis but appear to grow by exploiting the vessels present in the normal tissue.

The existence of these tumors has been predicted[7] but not previously identified. We have been able to demonstrate putative nonangiogenic tumors in the lung because of the unique structure of this organ, but their occurrence also in other tissues is likely. Lung parenchyma is made up of alveolar septa arranged in a highly regular pattern. The septa define empty spaces, the alveoli, which are filled with air. The task of this organ is to allow the exchange of gases between air and blood. Together with air, carbon particles present in pollution also reach the alveoli and accumulate in the alveolar walls, around the vessels, providing a unique *in vivo* labeling of these anatomical structures. When a nonangiogenic carcinoma develops, the neoplastic cells fill the alveoli without destroying the normal lung architecture, which survives "frozen" by the carcinoma and is easily recognized by its regular pattern. The presence of anthracytic pigment inside the alveolar walls, alongside the vessels, is a further suggestion that the only vessels observed are the normal ones. This supports the hypothesis that, if an appropriate vascular bed is available, a tumor can exploit it. Neoplastic cells without neovascularization filling the alveoli are a common finding on the edge of many lung tumors, but in the nonangiogenic tumors, this pattern is uniformly present throughout the whole tumor. This suggests that cells on the edge of the tumor commonly use existing vessels, but then in some tumors neoplastic cells switch to angiogenesis, whereas in other tumors, they do not.

Such a finding is not limited to primary carcinoma, but we also have noted that some metastatic carcinomas in the lung have the same appearance.[17]

These conclusions are based on morphology and raise two main questions. The first one is whether the neoplastic cells are truly in a nonangiogenic status, as suggested by the apparent lack of new vessel formation. Immunostaining of these tumors for angiogenic factors, such as vascular endothelial or platelet-derived growth factors, will be the next step. However, because anti-angiogenic factors cannot be demonstrated yet in such a way, functional and biochemical assays also will be necessary to fully characterize the angiogenic status of these tumors.

The second point concerns the vessels. A series of immunohistochemical studies, eg, looking at PECAM-1 or integrins, will be necessary to gather more information about the status of these vessels as far as activation, proliferation, and status of the surrounding stroma is concerned. All of these investigations are now being planned.

The angiogenic tumors destroy the lung parenchyma and elicit the formation of new stroma and vessels. The relationship among neoplastic cells, vessels, and epithelium has allowed us to identify three different patterns. In the papillary pattern, almost exclusively present in adenocarcinoma, cells exploit alveolar structures, but remodeling does invariably occur and the lung architecture is replaced by a papillary tumor growing along newly formed fibrovascular stalks. A peculiar distribution pattern of vessels comparable to the one we called basal was reported as mostly associated with squamous cell carcinomas by Yuan et al.[14] The same authors reported that in adenocarcinomas a different distribution pattern is present; vessels are mostly either around the neoplastic gland or in the stalk of the papillary structure, as we have reported in what we called the papillary pattern.

The arrangement of the tumor according to these vascular patterns is likely to reflect also several underlying biological differences. The angiogenic patterns are all likely to express proteases to destroy the normal parenchyma, growth factors to elicit tumor-associated stroma formation, and angiogenic factors. Furthermore, the basal and papillary patterns have still the capacity to reproduce the basic structure of a mucosa in which the epithelial cells lie over a supporting stroma in which the vessels are present, probably through the maintenance

Table 2. Characteristics of the Tumors According to the Vascular Patterns

	Angiogenic tumors			Nonangiogenic tumors	
	Basal	Papillary	Diffuse	Alveolar	*P* value
Number of cases	198	71	151	80	
Sex (M/F)	192/6	58/13	142/9	74/6	
% female	3%	18%	6%	7.5%	<0.0005*
Smokers	192	59	139	73	
Mean cigarettes/day	26.8	27.3	26.9	25.6	
Nonsmokers (%)	2 (1%)	10 (14.5%)	10 (6.7%)	3 (3.9%)	<0.0005*
Not known	4	2	2	4	
Disease-free	141	49	107	47	<0.05†
Metastases	46 (23.3%)	18 (25.3%)	36 (23.8%)	29 (36.3%)	<0.025†
Histiotype					
Adenocarcinoma	35 (17.7%)	59 (83%)	77 (51%)	39 (49%)	<0.0005*
Squamous cell carcinoma	152 (76.8%)	5 (7%)	54 (36%)	34 (48%)	
Others	11 (5.5%)	7 (10%)	20 (13%)	7 (9%)	
Grading (available on 447 cases only)					
Total	186	61	127	73	
Well differentiated	50 (27%)	37 (60.5%)	33 (26%)	4 (5.5%)	<0.0005*
Moderately differentiated	97 (52%)	18 (29.5%)	48 (38%)	36 (49.3%)	
Poorly differentiated	39 (21%)	6 (10%)	46 (36%)	33 (45.2%)	

**P* value calculated by the *r* × *c* frequency table.
†*P* value calculated using a 2 × 2 frequency table to compare all of the angiogenic *versus* the nonangiogenic tumors.

of complex systems mediated by adhesion molecules. Such ability is lost in the diffuse group where epithelial cells, stroma, and vessels are present but mixed up without any topographic order. The putative nonangiogenic carcinomas differ in many aspects and it will be of interest to compare proteases, growth factors, and angiogenic factors, which may be expressed only at basal levels or prevented from acting by the presence of inhibiting factors (eg, angiostatin). These tumors do not destroy the lung parenchyma and do not have tumor-associated stroma or new vessels.

The putative nonangiogenic tumors are highly aggressive,[18] and vessels could still play a key role. Their vascular density, due to the normal lung blood supply, is not higher than the other group but is likely to be more effective for several reasons. Locally, they can grow efficiently by exploiting the highly regular vascular network of the lung and progress by filling the empty alveolar spaces rather than destroying them and then building up new neoplastic tissue. Lung vessels also offer a vascular window[7] that can probably favor neoplastic spread. It remains to be seen whether these cells have angiogenic potential of their own or whether they rely on vessels present in other organs for growth of metastases. Certainly, they have a high metastatic potential and, in our series of 500 stage I cases, we have found that patients with these tumors have 25% more metastases than other patients, a figure that appears to have some statistical although weak meaning, as shown in Table 2. It is very likely that some of these cells acquire the ability to develop metastases infiltrating solid organs and then produce neo-angiogenesis.

The identification of these patterns could be the first step toward a new grading system of lung non-small-cell lung carcinoma. It has always been controversial whether the current grading system of lung tumors was of prognostic value.[30] As we have reported, there is a correlation between the papillary pattern and the well differentiated grade of tumor as defined currently, but we can split, as far as prognosis is concerned, the poorly differentiated into two types: the diffuse subtype, which is angiogenic, and the alveolar, which is likely to be nonangiogenic. Perhaps a combination of architecture and other prognostic markers easily identifiable and reproducible, such as mitotic rate, could lead to a grading system with prognostic value, similar to that already in use for breast cancer, which is based not only on nuclear atypia and number of mitoses but also on architectural parameters such as the ability to form glands.[31]

The identification and the investigation of the biological characteristics of these nonangiogenic tumors will be of paramount importance not only to better understand the origin of both primary and metastatic neoplasms but also for better planning of treatment. The possibility for clones

Table 3. Vascular Patterns and Tumor-Related Protein Expression

	Basal (positive/total)	Papillary (positive/total)	Diffuse (positive/total)	Alveolar (positive/total)	*P* value*
Bcl-2	19.5% (35/179)	5% (3/62)	6% (8/141)	24% (18/76)	<0.0005
p53	52% (100/193)	21% (14/67)	43% (61/143)	55% (43/78)	<0.0005
EGFR	53.5% (104/194)	32.5% (23/71)	53.5% (79/148)	43% (34/79)	<0.05
Laminin receptor	64% (127/198)	52% (37/71)	46% (69/151)	54% (43/80)	<0.005

**P* value calculated by *r* × *c* frequency tables.

Table 4. Summary of the Main Features According to the Vascular Patterns

	Angiogenesis patterns			
	Basal	Papillary	Diffuse	Alveolar
Mucosa architecture	Reproduced	Reproduced	Absent	Absent
Normal lung	Destroyed	Destroyed	Destroyed	Preserved
New vessels	Present	Present	Present	Absent
Tumor associated Stroma	Present	Present	Present	Absent
Non-smoker patients	Lower incidence	Higher incidence	Expected incidence	Expected incidence
Prevalent histiotype	Squamous	Adenocarcinoma	None	None
Prevalent grading	None	Well differentiated	Poorly differentiated	Poorly differentiated
Higher than expected number of cases positive for*	Bcl-2, laminin receptor			Bcl-2
Lower than expected number of cases positive for*		Bcl-2, p53, EGFR	Bcl-2, laminin receptor	

*As reported in Table 3.

without or with low angiogenic capacity to give origin to a clinical evident primary lung carcinoma suggests this type of disease will be resistant to treatment with anti-angiogenic drugs.

Acknowledgments

We thank Dr. Kingsley Micklem, Medical Informatics Unit, University Department of Cellular Science, Oxford, for his help in editing the artwork.

References

1. Folkman J: Tumour angiogenesis: therapeutic implication. N Engl J Med 1971, 285:1182–1186
2. Folkman J: What is the evidence that tumours are angiogenesis dependent? J Natl Cancer Inst 1990, 82:4–6
3. Blood CH, Zetter BR: Tumor interactions with the vasculature: angiogenesis and tumour metastasis. Biochem Biophys Acta 1990, 1032:89–118
4. Hart IR, Saini A: Biology of tumour metastasis. Lancet 1992, 339: 1453–1457
5. Ellis LM, Fidler IJ: Angiogenesis and metastasis. Eur J Cancer 1996, 32A:2451–2460
6. Weidner N: Tumour angiogenesis: review of current applications in tumour prognostication. Semin Diagn Pathol 1993, 10:302–313
7. Weidner N: Intratumor microvessel density as a prognostic factor in cancer. Am J Pathol 1995, 147:9–19
8. Gasparini G, Harris AL: Clinical importance of the determination of tumor angiogenesis in breast carcinoma: much more than a new diagnostic tool. J Clin Oncol 1995, 13:765–782
9. Craft PS, Harris AL: Clinical prognostic significance of tumour angiogenesis. Ann Oncol 1994, 5:305–311
10. Leedy DA, Trune DR, Kronz JD, Weidner N, Cohen JI: Tumor angiogenesis, the p53 antigen and cervical metastasis in squamous carcinoma. Otolaryngol Head Neck Surg 1994, 111:417–422
11. Fontanini G, Bigini D, Vignati S, Basolo F, Mussi A, Lucchi M, Chine S, Angeletti CA, Harris AL, Bevilacqua G: Microvessel count predicts metastatic disease and survival in non-small cell lung cancer. J Pathol 1995, 177:57–63
12. Giatromanolaki A, Koukourakis M, O'Byrne K, Fox S, Whitehouse R, Talbot D, Harris AL, Gatter KC: Angiogenesis is a significant prognostic marker in operable non-small cell lung cancer. J Pathol 1995, 179:80–88
13. Yamazaki K, Abe S, Takekawa H, Sukoh N, Watanabe N, Ogura S, Nakajima I, Isobe H, Inoue K, Kawakami Y: Tumor angiogenesis in human lung adenocarcinoma. Cancer 1994, 74:2245–2250
14. Yuan A, Yng PC, Yu CJ, Lee YC, Yao YT, Chen CL, Lee LN, Kuo SH, Luh KT: Tumour angiogenesis correlates with histologic type and metastasis in non-small cell lung cancer. Am J Respir Crit Care Med 1995, 152:2157–2162
15. Macchiarini P, Fontanini G, Hardin MJ, Squartini F, Angeletti CA: Relation of neovascularisation to metastasis of non small cell lung cancer. Lancet 1992, 340:145–146
16. Macchiarini P, Fontanini G, Dulmet E, de Montpreville V, Chapelier AR, Cerrina J, Ladurie FL, Dartevelle PG: Angiogenesis: an indicator of metastasis in non-small cell lung cancer invading the thoracic inlet. Ann Thorac Surg 1994, 57:1534–1539
17. Pezzella F, Di Bacco A, Andreola S, Nicholson AG, Pastorino U, Harris AL: Angiogenesis in primary lung cancer and lung secondaries. Eur J Cancer 1996, 32A:2494–2500
18. Pastorino U, Andreola S, Tagliabue E, Pezzella F, Incarbone M, Sozzi G, Buyse M, Menard S, Pierotti M, Rilke F: Immunocytochemical markers in stage I lung cancer (NSCLC): relevance to prognosis. J Clin Oncol 1997, 15:2858–2865
19. Mountain CF: A new international staging for lung cancer. Chest 1986, 89:225–233
20. Anonymous: The World Health Organization histological typing of lung tumours. Am J Clin Pathol 1982, 77:123–136
21. Colby TV, Koss MN, Travis WD: Tumours of the lower respiratory tract. Anonymous Atlas of Tumor Pathology. Washington, DC, Armed Force Institute of Pathology, 1994
22. Parums DV, Cordell JL, Micklem K, Heryet AR, Gatter KC, Mason DY: JC70: a new monoclonal antibody that detects vascular endothelium associated antigen on routinely processed tissue sections. J Clin Pathol 1990, 43:752–757
23. Martignone S, Pellegrini R,, Villa E, Tandon NN, Mastrolanni A, Tagliabue E, Menard S, Colnaghi MI: Characterization of two monoclonal antibodies directed against the 67 kd high affinity laminin receptor and applications for the study of breast carcinoma progression. Clin Exp Metastasis 1992, 10:389–396
24. Pezzella F, Tse A, Cordell JL, Pulford KAF, Gatter KC, Mason DY: Expression of the bcl-2 protein is not specific for the 14;18 chromosomal translocation. Am J Pathol 1990, 137:225–232
25. Cattoretti G, Pileri S, Parravicini C, Becker MH, Poggi S, Biculco C, Key G, D'Amato L, Sabattini E, Feudale E, Reynolds F, Gerdess J, Rilke F: Antigen unmasking of formalin-fixed, paraffin embedded tissue sections. J Pathol 1993, 171:83–98
26. Fox SB, Leek RD, Weekes MP, Whitehouse RM, Gatter KC, Harris AL: Quantitation and prognostic value of breast cancer angiogenesis: comparison of microvessel density, Chalkley count and computer image analysis. J Pathol 1995, 177:275–283
27. Altman DG: Practical Statistics for Medical Research. London, Chapman and Hall, 1991
28. Paakko P, Risteli J, Risteli L, Autio-Harmainen H: Immunohistochemical evidence that lung carcinomas grow on alveolar basement membranes. Am J Surg Pathol 1990, 14:464–473
29. Mackay B, Leukeman JM, Ordonez NG: Tumors of the lung. Philadelphia, WB Saunders, 1991, pp 165–189
30. Carriaga MT, Henson DE: The histologic grading of cancer. Cancer 1995, 75:406–421
31. Elston CW, Ellis IO: Pathologic prognostic factors in breast cancer. I. The value of histological grade in breast cancer: experience from a large study with long term follow-up. Histopathology 1991, 19:403–410

Angiogenesis-independent tumor growth mediated by stem-like cancer cells

Per Ø. Sakariassen[a], Lars Prestegarden[a], Jian Wang[a], Kai-Ove Skaftnesmo[a], Rupavathana Mahesparan[a,b], Carla Molthoff[c], Peter Sminia[d], Eirik Sundlisæter[a], Anjan Misra[e], Berit Bølge Tysnes[a], Martha Chekenya[a], Hans Peters[f], Gabriel Lende[b], Karl Henning Kalland[g,h], Anne M. Øyan[g,h], Kjell Petersen[i], Inge Jonassen[i,j], Albert van der Kogel[f], Burt G. Feuerstein[k], A. Jorge A. Terzis[a,l], Rolf Bjerkvig[a,l], and Per Øyvind Enger[a,b,m]

[a]NorLux NeuroOncology, Department of Biomedicine, University of Bergen, N-5020 Bergen, Norway; Departments of [b]Neurosurgery and [c]Microbiology and Immunology, Haukeland University Hospital, N-5021 Bergen, Norway; Departments of [e]Nuclear Medicine and Positron Emission Tomography Center and [d]Radiation Oncology, Section Radiobiology, Vrije Universiteit University Medical Center, 1081 HV Amsterdam, The Netherlands; Departments of [e]Neurosurgery and [k]Laboratory Medicine, University of California, San Francisco, CA 94143; [f]Department of Radiation Oncology, University Medical Center, 6500 HB Nijmegen, The Netherlands; [g]The Gade Institute, University of Bergen, N-5021 Bergen, Norway; [h]Bergen Center for Computational Science, Unifob A/S and [i]Department of Informatics, University of Bergen, N-5021 Norway; and [l]NorLux Neuro-Oncology, Centre Recherche de Public Santé, L-1150 Luxembourg

Communicated by Erkki Ruoslahti, University of California, Santa Barbara, CA, September 1, 2006 (received for review May 5, 2006)

In this work, highly infiltrative brain tumors with a stem-like phenotype were established by xenotransplantation of human brain tumors in immunodeficient nude rats. These tumors coopted the host vasculature and presented as an aggressive disease without signs of angiogenesis. The malignant cells expressed neural stem cell markers, showed a migratory behavior similar to normal human neural stem cells, and gave rise to tumors *in vivo* after regrafting. Serial passages in animals gradually transformed the tumors into an angiogenesis-dependent phenotype. This process was characterized by a reduction in stem cells markers. Gene expression profiling combined with high throughput immunoblotting analyses of the angiogenic and nonangiogenic tumors identified distinct signaling networks in the two phenotypes. Furthermore, proinvasive genes were up-regulated and angiogenesis signaling genes were down-regulated in the stem-like tumors. In contrast, proinvasive genes were down-regulated in the angiogenesis-dependent tumors derived from the stem-like tumors. The described angiogenesis-independent tumor growth and the uncoupling of invasion and angiogenesis, represented by the stem-like cancer cells and the cells derived from them, respectively, point at two completely independent mechanisms that drive tumor progression. This article underlines the need for developing therapies that specifically target the stem-like cell pools in tumors.

glioma | invasiveness | vessel cooption

A basic principle in tumor progression is the requirement for angiogenesis, yet several clinical studies have reported limited efficacy of angiogenesis inhibitors to control tumor growth (1–7). This finding has been explained by pharmacokinetic parameters such as the mode of delivery, inadequate biodistribution, and misfolding of the therapeutic proteins (8). Still, some studies suggest that the nature of this problem may not be inherent in the therapeutic compound, but rather underlies the concept of angiogenesis-dependency itself (9–11). An alternative mechanism for obtaining essential nutrients may be that the malignant cells are sustained by the preexisting vasculature of the host tissue, as they invade the surrounding parenchyma.

Stem cells and tumor cells share the ability of cell division. Moreover, EGF and FGF, which maintain neural stem cells in a proliferative state *in vitro*, also increase proliferation of glioma cells (12–14). Similar to migrating neural stem cells grafted in adult rat brain, invading glioma cells may be supported by the vascular network in the normal brain (15–19). However, studies suggest that although tumor cells initially coopt surrounding vessels, subsequent growth requires angiogenesis (20, 21). Thus, the prevailing view is that solid tumor growth is angiogenesis-dependent (22–24).

Glioblastomas (GBMs) are highly vascular brain tumors that are considered to be attractive candidates for antiangiogenic therapy (25). GBMs are classified as high-grade gliomas because of the presence of necrosis and microvascular proliferations, and most often arise *de novo* in patients not previously diagnosed with a low-grade glioma. They are then referred to as primary GBMs and display a characteristic set of genetic changes (26, 27). However, these tumors may also arise from the malignant progression of invasive, low-grade gliomas without microvascular proliferations (26, 28). Apart from the onset of angiogenesis, this transition is characterized by progressive genetic changes different from those observed in primary GBMs (29). In this work, we xenografted 10 biopsies from primary glioblastomas into nude rat brains. Surprisingly, the resulting tumors recapitulated the infiltrative growth pattern of low-grade gliomas, coopting the host vasculature without any signs of angiogenesis or necrosis. Upon passaging *in vivo*, they progressed toward a highly malignant phenotype displaying tumor angiogenesis and large necrotic regions. This progression was not

Table 1. Tumor take, engraftment rate, and passaging data on 10 primary GBM biopsies

Case	Tumor take (%)	Survival, days, mean ± SEM*	Passaged *in vivo*
1	12 of 13 (92)	117.5 ± 8.6	No
2	7 of 7 (100)	97 ± 1.7	Yes
3	4 of 5 (80)	169.5 ± 22.1	No
4	3 of 5 (60)	252 ± 1.6	No
5	7 of 8 (88)	64 ± 1.5	No
6	2 of 10 (20)	93.5 ± 10.6	No
7	6 of 6 (100)	104.5 ± 1.4	Yes
8	8 of 8 (100)	119.5 ± 3.5	Yes
9	12 of 14 (86)	137.5 ± 5	No
10	7 of 7 (100)	126.5 ± 2.9	Yes

*Survival data were recorded only from animals where tumor take was confirmed after histological examination.

Author contributions: P.Ø.S. and L.P. contributed equally to this work; P.Ø.S., L.P., R.M., G.L., B.G.F., R.B., and P.Ø.E. designed research; P.Ø.S., L.P., J.W., K.-O.S., R.M., C.M., P.S., E.S., A.M., H.P., K.H.K., A.M.Ø., A.v.d.K., and P.Ø.E. performed research; C.M., P.S., and H.P. contributed new reagents/analytic tools; P.Ø.S., L.P., J.W., K.-O.S., A.M., B.B.T., M.C., H.P., K.H.K., A.M.Ø., K.P., I.J., B.G.F., A.J.A.T., R.B., and P.Ø.E. analyzed data; and P.Ø.S., L.P., R.B., and P.Ø.E. wrote the paper.

The authors declare no conflict of interest.

Freely available online through the PNAS open access option.

Abbreviations: CGH, comparative genomic hybridization; GBM, glioblastoma.

[m]To whom correspondence should be addressed at: Department of Biomedicine/SAC, University of Bergen, Jonas Lie's Vei 91, 5009 Bergen, Norway. E-mail: per.enger@biomed.uib.no.

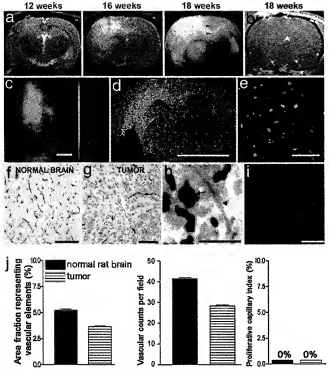

Fig. 1. Tumor growth without angiogenesis. (*a*) MRI scans (T_2 sequence) at three different time points. The midline structure at 18 weeks, as indicated by arrowheads. (*b*) T_1 sequence after gadodiamid administration. (*c*) A [^{18}F]FLT positron emission tomography scan of a rat brain with a tumor. (*d*) Coronary rat brain section costained with BrdU (green) and collagen IV (red). (*e*) Triple staining of the tumor bed for BrdU (green), collagen IV (red), and Hoechst (blue). (*f*) CD31 staining of vessels in the normal brain. (*g*) CD31 staining of vessels in the tumor. (*h*) Costaining for von Willebrand factor (red) and Ki67 (brown). Ki67-positive tumor cell nucleus (arrow), and Ki67-negative endothelial nucleus (arrowhead) are shown. (*i*) Double staining for collagen IV (red) and pimonidazol (green). (*j*) Morphometric quantification of vascular parameters in the first-generation tumors and in the normal brain. Error bars show SEM. [Scale bars: 1 cm (*c* and *d*); 100 μm (*e–g*); 40 μm (*h*); and 5 mm (*i*).]

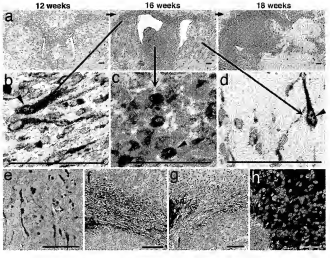

Fig. 2. Nonangiogenic tumors contain cells with stem-like features. (*a*) Brain sections at different time points corresponding to the MRI scans. The main tumor mass has a purple color because of immunostaining with a human-specific antibody against vimentin. Costaining with anti-human vimentin (red) and Ki67 (brown) show dividing and nondividing tumor cells in different regions of the brain: corpus callosum (*b*), tumor bulk (*c*), and contralateral hemisphere (*d*). (*e*) Nestin-positive cancer cells (brown) invading the parenchyma in the contralateral hemisphere. (*f* and *g*) Migration along corpus callosum of vimentin-positive cancer cells (brown) from a tumor spheroid (*f*) and of human neural stem cells (*g*). (*h*) Musashi-1-positive cells (green) migrating from a tumor spheroid (red). (Scale bars: 50 μm.)

paralleled by progressive genetic derangements because the angiogenic and nonangiogenic phenotypes had almost identical array comparative genomic hybridization (CGH) profiles. However, they displayed distinct gene-expression profiles, suggesting that transcriptional modulation mediated the phenotypic shift. Our findings demonstrate that even highly vascular and aggressive tumors, with no definable precursor lesions, contain tumor cells that can revert and adapt the growth characteristics of low-grade tumors. Subsequently, these tumors can again progress to become vascular and necrotic. Our results show that the cellular heterogeneity and adaptive behavior demonstrated by these tumor cells bears a resemblance to the plasticity of stem cells and implies that anti-angiogenic cancer therapy should be combined with a therapy that targets the invasive stem-like cell populations.

Results

Patient Characteristics, Immunohistochemistry, and Engraftment Rate of Tumor Biopsies and Glioma Spheroids. Spheroids derived from biopsy tissue of 10 patients with GBM all developed tumors (hereafter termed first-generation tumors) when transplanted into the CNS of nude rats (30, 31), although at varying rates (Table 1). All tumors were previously untreated, primary glioblastomas, with histological features defined by nuclear pleomorphism, mitosis, necrosis, and endothelial cell proliferation (Fig. 6*a*, which is published as supporting information on the PNAS web site). The tissue specimens were minced and cultured *in vitro* in serum containing medium to form glioma spheroids before implantation (Fig. 6 *Right*). Immunohistochemical staining displayed a strong expression of glial fibrillary acidic protein (GFAP) both in the tumor biopsies and the biopsy spheroids (Fig. 6*b*), whereas nestin was up-regulated in the spheroids (Fig. 6*c*). The tumor biopsies showed some staining for the cancer stem cell marker CD133, in contrast to the spheroids, which were CD133 negative (Fig. 6*d*).

Highly Vascular Brain Tumors Contain Cancer Cells with the Capacity to Generate New Tumors Without Angiogenesis. To study tumor progression, we used longitudinal MRI over three time points (Fig. 1*a*). The T_2 scans displayed diffuse lesions that occupied most of the hemispheres in the terminal stage, causing a shift of midline structures. Although engraftment took place from all of the biopsies, the xenografts from seven patients developed without signs of contrast enhancement (Fig. 1*b*). For two biopsies, only minor enhancement was visible, and only one biopsy developed into a tumor with contrast enhancement (data not shown). Animals displaying no contrast enhancements were subsequently infused with ^{18}F-3′-deoxy-3′-fluorothymidine ([^{18}F]FLT) and examined by positron emission tomography (32). The scans showed a diffuse intracranial uptake of [^{18}F]FLT, indicating a disseminated spread of dividing tumor cells throughout the brain (Fig. 1*c*). Similarly, brain sections from rats pulsed with BrdU before killing, showed BrdU-positive cells spreading over the corpus callosum to the contralateral hemisphere (Fig. 1*d*). Moreover, we performed triple staining for the basement membrane marker collagen IV and BrdU in rats systemically injected with Hoechst 33342 (Fig. 1*e*). BrdU-positive cells were observed between blood vessels with no Hoechst leakage into the surrounding parenchyma, suggesting a normal vascular morphology and a functionally intact blood–brain barrier. Immunostaining and morphometric quantification for the vascular marker CD31 revealed that the area fraction representing vascular elements and vascular counts per field was slightly lower in the tumors compared with the normal brain (Fig. 1*f*, *g*, and *j*). This

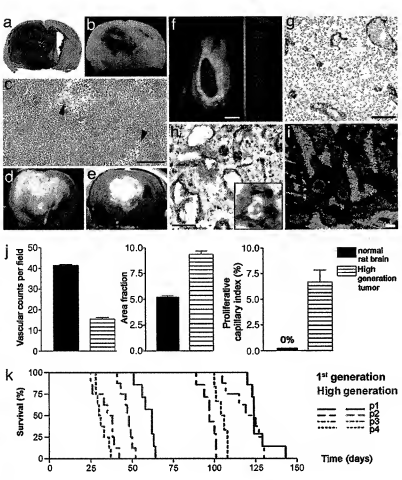

Fig. 3. Angiogenesis-independent stem-like tumors progress to become vascular and necrotic tumors. (*a*) H&E staining of a high-generation tumor. Dashed lines indicate the tumor periphery. (*b*) Picture of the same tumor exhibiting macroscopic necrosis (arrowhead). (*c*) H&E staining of a high-generation tumor at high magnification with enlarged vessels and arrowheads indicating necrotic areas. (*d* and *e*) T_2-weighted (*d*) and gadodiamid-enhanced T_1-weighted (*e*) MRI scans of a high-generation tumor. White area in e represents contrast enhancement. (*f*) Positron emission tomography scan of the rat brain tumor. (Scale bar: 1 cm.) (*g*) CD31 staining (brown) of the tumor bed. (*h*) Costaining for von Willebrand (red) and Ki67 (brown). (*Inset*) Proliferating endothelial cells (arrowheads). (*i*) Triple staining of a tumor section against pimonidazol (green), collagen IV (red), and Hoechst (blue). (*j*) Quantification of vascular parameters and comparison with normal brain. (*k*) Kaplan–Meyer curves presenting survival data for animals grafted with four patient biopsies that were passaged from first- to high-generation. (Scale bars: 100 μm, unless otherwise indicated.)

result may be attributed to cells infiltrating the vascular bed, thereby increasing the distance between neighboring vessels. Double staining for Ki67 and von Willebrand factor showed dividing tumor cells among quiescent normally sized blood vessels (Fig. 1*h*). No dividing endothelial cells were observed in the tumors. Double staining for collagen IV and the hypoxia marker pimonidazol revealed no sign of hypoxia in the first-generation tumor (Fig. 1*i*). Sections of rat brains perfused with India ink (Fig. 7*a*, which is published as supporting information on the PNAS web site) and transmission electron microscopy (Fig. 7*b*) also revealed a normal endothelial morphology and tight junctions between the endothelial cells. Immunohistochemical detection of reactive endothelial cells by staining for angiopoietin-2 was negative (Fig. 8*a*, which is published as supporting information on the PNAS web site).

Angiogenesis-Independent Growth Is Mediated by Tumor Cells That Exhibit Stem-Like Characteristics. Rat brains harvested at the time of MRI (Fig. 1*a*) allowed comparison with histological sections from corresponding regions (Fig. 2*a*). In all regions of the brain, we identified Ki67-positive tumor cells, which also stained positive for human-specific vimentin, a marker present in neuroepithelial progenitors and stem cells (33) (Fig. 2 *b–d*). Tumor cells migrating along the corpus callosum, entering the cortex, also expressed the neural stem cell marker nestin (Fig. 2*e*). For comparison, transplanted glioma spheroids and human neural stem cells (HNSC 100) were stained for vimentin and showed a striking similarity in their migratory pattern (Fig. 2 *f* and *g*). The tumor cells also expressed the neural stem cell marker musashi-1 (Fig. 2*h*), an RNA-binding protein involved in asymmetric cell division during *Drosophila* neural development (34).

Serial Passaging *in Vivo* Changes the Nonangiogenic Tumor to a Highly Vascular Phenotype. To further investigate tumor progression, first-generation tumors from four patients (Table 1) were removed and serially passaged in rats for 4–5 generations (hereafter termed high-generation tumors). In the subsequent generations, the tumors became more vascular and circumscribed (Fig. 3*a*) with emerging necrotic regions (Fig. 3 *b* and *c*). Moreover, MR1 scans showed less invasive (Fig. 3*d*), strongly contrast-enhancing tumors (Fig. 3*e*) in the high generation. The less-invasive nature of the high-generation tumors was also confirmed by positron emission tomography scans, where they appeared sharply demarcated (Fig. 3*f*). Immunohistochemistry revealed tumors with a disordered vasculature, dilated vessels, and endothelial cell proliferations (Fig. 3 *g* and *h*). Triple staining for collagen IV and the hypoxia marker pimonidazole in rats infused with Hoechst 33342 revealed numerous hypoxic areas surrounded by dilated vessels with Hoechst leakage into the surrounding parenchyma (Fig. 3*i*). This leakage was also confirmed in rats that had received systemic injections of India ink (data not shown). A morphometric quantification of the vascular parameters (Fig. 3*j*) revealed lower vascular counts per visual field in the high-generation tumors compared with normal rat brain, whereas the area fraction representing endothelial cells per visual field was increased. Finally, the proliferative capillary index was 6% in the tumors compared with 0% in the normal brain. The onset of angiogenesis coincided with a significant decrease in survival from 113 ± 2.6 SEM to 43 ± 2.1 SEM days (Fig. 3*k*).

Angiogenesis-Independent and -Dependent Phenotypes Are Genetically Similar, but Display Different Gene and Protein Expression Profiles and Distinct Patterns of Intracellular Signaling. Array CGH showed that the human biopsy and the first- and high-generation

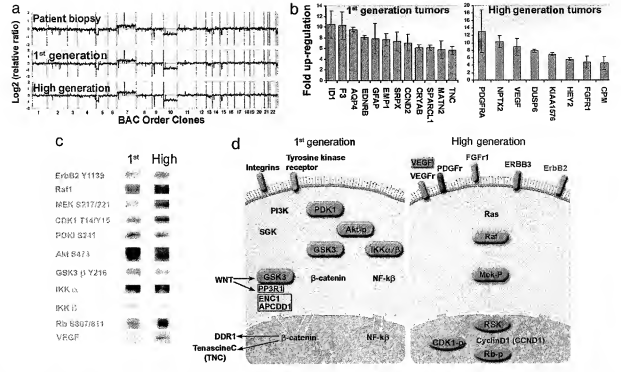

Fig. 4. Comparison of chromosomal DNA, gene expression, and protein profiles between first- and high-generation tumors. (*a*) Array CGH showing the relative chromosome copy numbers of the parent biopsy, first- and high-generation tumors. (*b*) Bar graph presenting the genes with the biggest difference in expression levels between the first- and high-generation tumors. (*c*) Immunoblot analysis of protein extracts from first- and high-generation tumor tissue. VEGF was analyzed from cerebrospinal fluid. (*d*) Signaling pathways differentially activated in the two tumor phenotypes.

tumors displayed nearly identical chromosomal profiles (Fig. 4*a*), where they showed loss on chromosome 5p, gain on 7 with EGFR amplification, INK4A/ARF homozygous deletion, loss of chromosome 10, and interstitial loss of 15q. The striking similarities in the array CGH profiles between the tumors suggested that transcriptional regulation is an important component in the phenotypic shift observed. Therefore, a comprehensive gene-expression analysis comparing first- and high-generation tumors was performed. In total, we found 77 genes whose differential expression was 2-fold or more between the two tumor phenotypes, using three different microarray platforms [16,000-oligonucleotide cDNA; Agilent Technologies (Palo Alto, CA), 44,000-oligonucleotide; Agilent Technologies, and 37,000-oligonucleotide microarrays; Applied Biosystems (Foster City, CA)] (Fig. 4*b*, and Table 2, which is published as supporting information on the PNAS web site). Furthermore, two of the array platforms contained vimentin and nestin, which where up-regulated 200% and 70% in the first-generation, respectively. To ensure that this up-regulation was human-specific and not caused by reactive host-derived cells, we designed primers specific for rat vimentin. Quantitative real-time PCR (RT-qPCR) from low- and high-generation confirmed that the expression was from the tumor cells (Fig. 9, which is published as supporting information on the PNAS web site). Moreover, a comprehensive Kinetworks multimmunoblotting screen was performed, which represents a systems-biology approach providing simultaneous expression and phosphorylation states of hundreds of target proteins. The Kinetworks screen revealed numerous proteins to be differentially expressed, including main components of intracellular signaling pathways (Fig. 4*c*). Based on the gene-expression profiles and the Kinetworks screen, we found that components of the Wnt, PI3K, and NF-kβ signaling pathways were overexpressed in the invasive first-generation tumors compared with the high-generation tumors. In addition, although components of the Ras signaling pathway were expressed in both first- and high-generation tumors, they were significantly up-regulated in the high generation (Fig. 4*d*). Moreover, the first-generation tumors displayed up-regulation of genes involved in fetal development and cell motility (Table 3, which is published as supporting information on the PNAS web site).

Invasion and Angiogenesis, Two Independent Strategies for Tumor Progression. The tumor cell invasion marker SPARC (35–37) was up-regulated in first-generation tumors, whereas the high-generation tumors displayed weak or no staining (Fig. 5*a*). Furthermore, spheroids from first-generation tumors were highly invasive when tested in a collagen-invasion-gel assay, whereas the high-generation tumor spheroids only displayed a modest invasion in the gel (Fig. 5*b*).

Conversely, immunostaining for HIF-1α and VEGF were negative in sections from first-generation tumors, whereas staining for both markers were positive in the high-generation tumors (Fig. 5 *c* and *d*). The same staining pattern was seen for angiopoitin-2 (Fig. 8). Furthermore, Western blotting for HIF-1α and quantitative real-time PCR (RT-qPCR) for its target gene carbon anhydrase IX (CAIX) showed up-regulation in the high-generation tumors, whereas RT-qPCR for VEGF in the first-generation tumors showed levels comparable with normal brain (Fig. 10 *a–c*, which is published as supporting information on the PNAS web site). In addition, HIF-1α was not detected in tumor spheroids in normoxic conditions but was up-regulated in hypoxia, followed by an increase of CAIX expression (Fig. 11 *a* and *b*, which is published as supporting information on the PNAS web site). Moreover, we functionally assessed the angiogenic potential of first- and high-generation tumors in a rat aortic ring assay (Fig. 5*e*). Endothelial cell sprouting was evident only from aortic rings that received conditioned medium from high-generation tumor spheroids. Conditioned media from first-generation tumor spheroids induced no outgrowth of endothelial cells during the observation period of 11 days, suggesting that first-generation tumors do not secrete the necessary amounts of angiogenic factors to trigger angiogenesis.

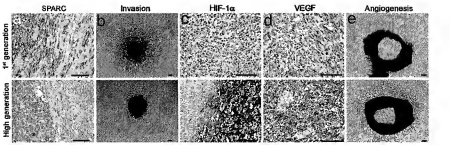

Fig. 5. Inverse relationship between angiogenesis and invasion. (*a*) SPARC immunostaining (brown) at the tumor periphery in first- and high-generation tumors. (*b*) Invasion of tumor cells in a collagen gel from first- and high-generation glioma spheroids. (*c* and *d*) Hif-1α and VEGF expression (brown), respectively, in first- and high-generation tumors. (*e*) Aortic ring explants incubated with conditioned medium from first- and high-generation tumor spheroids. Pictures from aortic ring and collagen-invasion assays were all taken on day 5. (Scale bars: 100 μm.)

Discussion

Malignant gliomas are the most common cancers in the brain and remain difficult to cure despite advances in surgery and adjuvant therapy. Recent studies have identified tumor cell subpopulations that might be responsible for tumor initiation and progression. Cancer stem cells have been identified in leukemias and breast, prostate, and brain cancer (38–44). In some cases, these tumor-initiating cells can be distinguished from the non-tumor-initiating cancer cells based on cell surface marker expression. For instance, it has been found that only $CD44^+/CD24^-/lineage^-$ breast cancer cells form new tumors in animals (45). Similarly, CD133 has been proposed as a cancer stem cell marker in brain cancers (46). However, we established tumors *in vivo* from GBM-derived spheroids that contained $nestin^+/GFAP^+/CD133^-$ cells. This discrepancy may be due to different culture conditions because we cultured our biopsy material in serum-containing medium. The implanted tumor spheroids developed tumors with a stem-like, nonangiogenic and highly invasive phenotype. The first-generation tumors mediated a fulminant fatal disease course, and 7 of 10 specimens produced this phenotype. Two other specimens developed into highly invasive tumors with a predominantly normal vasculature, and only one biopsy produced contrast enhancement. Although the cellular program mediating the nonangiogenic phenotype is possibly a remnant of fetal development that lies dormant during normal tumorigenesis, the program may be reactivated to drive tumor progression in a clinical setting when patients are treated with angiogenic inhibitors. In contrast to the dormant tumors that become malignant only after the onset of angiogenesis (21), our results challenge the current view of malignant tumor growth as an angiogenesis-dependent process.

Despite the fact that the nonangiogenic phenotype recapitulates developmental signaling pathways and expresses stem cell markers, it is not clear whether these cells are derived from transformed neural stem cells, from stem cell fusion events (47), or from otherwise restricted subpopulations within the tumor. The genetic similarities between the different tumor phenotypes, as demonstrated by almost identical array CGH profiles, do not support a major involvement of clonal selection, but suggest that transcriptional regulation mediates the phenotypes observed. Furthermore, it has been shown that an astrocytoma cell line became more invasive after knocking out the *HIF-1α* gene (48).

In later generations, transition to a vascular tumor phenotype is mediated by cells where the Ras-signaling pathway is activated. Thus, the capacity for tumor growth is neither limited to a genetic subclone nor to a certain cell phenotype, but is shared between groups of phenotypically diverse cells, where some are characterized by a diffuse growth pattern and others by angiogenesis. Accordingly, the uncoupling of invasion and angiogenesis, represented by the stem-like cancer cells and the cells derived from them respectively, points at two different mechanisms that drive tumor progression. Although the mechanism behind the phenotypic shift is not fully understood, HIF-1α expression seems to be triggered by hypoxia, because it was not constitutively expressed by high-generation tumor spheroids cultured under normoxic conditions. The results showing that both phenotypes can mediate a fulminant disease course suggest that even a 100%-effective therapy directed toward one of the biological entities (either invasion or angiogenesis) will not cure the cancer. Cancer treatment strategies need to pursue both the invasive stem-like cancer cells and angiogenic targets. A major challenge will be to design therapies that target the stem-like cancer cells without destroying the normal stem cell pools that are needed to maintain normal tissue function.

Materials and Methods

Cell Culture and *in Vitro* Assays. Biopsy spheroids were prepared as described (49). After 1–2 weeks in culture, spheroids with diameters between 200 and 300 μm were selected for intracerebral implantation.

***In Vivo* Experiments.** Nude immunodeficient rats (Han: rnu/rnu Rowett) were fed a standard pellet diet and were provided with water ad libitum. All procedures were approved by The National Animal Research Authority. Biopsy spheroids were stereotactically implanted into the right brain hemisphere, and the rats were killed when symptoms developed.

Immunohistochemistry. After deparaffinization, all sections were boiled in citrate buffer, pH 6.2, for 20 min, except for the von Willebrand staining, where the sections were treated with proteinase K (DAKO, Glostrup, Denmark) for 10 min. Sections were then treated with protein-blocking solution (DAKO) for 10 min, and the primary antibody was incubated for 45 min at room temperature, washed four times, incubated for 35 min with En Vision+ Systems polymer-conjugated secondary antibody (DAKO), washed four times, and finally incubated with DAB for 5 min.

Transmission Electron Microscopy. The rats were perfusion fixed, and the brains were removed and embedded in Epon 812, followed by ultrathin sectioning in preparation for electron microscopy.

Hypoxia Experiment. Spheroids were cultured at 37°C with 5% CO_2, 94% N_2, and 1% O_2 for 16 h in a Mini Galaxy incubator (RS Biotech, Ayrshire, Scotland, U.K.).

Western Blotting. Cerebrospinal fluid was run on SDS/PAGE by using NuPage precast gels (Invitrogen, Carlsbad, CA). After blotting, the nitrocellulose membrane was blocked for 30 min at room temperature and incubated overnight at 4°C in buffer (TBS with 0.1% Tween 20, 5% milk powder) containing anti-VEGF-A diluted

1:100 (Abcam, Cambridge, U.K.), anti-HIF1α diluted 1:100 (BD Biosciences, San Diego, CA), or anti-GAPDH diluted 1:2,000 (Abcam). The primary antibody was detected by using an HRP-conjugated goat anti-rabbit/mouse secondary antibody (Immunotech, Fullerton, CA) diluted 1:2,500. Extraction of protein from cultured spheroids was done by washing in PBS two times and homogenizing in lysis buffer by sonication twice for 15 sec by using Sonics Vibra Cell (Cole–Parmer Instruments, Vernon Hills, IL). Whole lysate was used for subsequent analysis. Twenty micrograms of protein was applied in each well.

Protein Kinase and Phosphosite Screening. The procedure is described in refs. 50 and 51. The following screens were performed: KPKS-1.2A, KPKS-1.2B, KPSS-2.1, KPSS-4.1, and KPSS-1.3. For details, see the Kinexus (Advent Software, San Francisco, CA) home page www.kinexus.com.

Quantitative RT-PCR. cDNA was generated by using the iScript cDNA synthesis kit according to the manufacturers instructions (Bio-Rad, Hercules, CA). Each reaction is in triplicate on the plate, and a similar plate was repeated three times. The reactions were performed by using iQ SYBR green Supermix reagents kit (Bio-Rad), and the PCR was run on a BioRad iCycle detection system (Bio-Rad).

Gene-Expression Analysis. Single-stranded cDNA was reverse transcribed from 2 μg of total RNA and T7 RNA polymerase promoter-containing double-stranded cDNAs, and T7 RNA polymerase-amplified RNAs (cRNAs) were generated according to the T7 Megakit protocol (Ambion, Austin, TX) as described (52).

Agilent DNA Microarrays. The Agilent 16,000-oligonucleotide cDNA microarrays were processed as described (53).

ABI1700 DNA Oligonucleotide Microarrays. The Human Genome Survey Microarray, Chemiluminescence Detection kit, Applied Biosystems Chemiluminescent RT-IVT Labeling kit, and Applied Biosystems 1700 Chemiluminescent Microarray Analyzer was used as recommended.

Bioinformatic Analysis of DNA Microarray Data. In total, six hybridizations were performed, two for each platform. The result files from the three different image-processing software programs were all imported into the analysis software J-Express (54). Controls and flagged spots were removed. J-Express is available at www.molmine.com.

Array CGH. To determine the copy number across all chromosomes, we did comparative genomic hybridizations on whole-genome arrays of 2,400 chromosomally mapped BAC clones (Hum. Array1.14) following methods described in ref. 55.

Supporting Information. For more information, see *Supporting Materials and Methods*, which is published as supporting information on the PNAS web site.

We thank Aina Johannessen, Linda Vabø, and Tore-Jacob Raa for technical assistance. This work was supported by the Norwegian Cancer Society, the Norwegian Research Council, Innovest AS, Helse-Vest, Haukeland University Hospital, the Bergen Translational Research Program, the Centre Recherche de Public Santé Luxembourg, and the European Commission 6th Framework Program Contract 504743.

1. Eisterer W, Jiang X, Bachclot T, Pawliuk R, Abramovich C, Leboulch P, Hogge D, Eaves C (2002) *Mol Ther* 5:352–359.
2. Gerber K (2002) *Nat Biotechnol* 20:1067–1068.
3. Brem S, Grossman SA, Carson KA, New P, Phuphanich S, Alavi JB, Mikkelsen T, Fisher JD (2005) *Neuro-oncol* 7:246–253.
4. Akella NS, Twiggs DB, Mikkelsen T, Hochberg FH, Grossman S, Cloud GA, Nabors LB (2004) *J Magn Reson Imaging* 20:913–922.
5. Gagner JP, Law M, Fischer I, Newcomb EW, Zagzag D (2005) *Brain Pathol* 15:342–363.
6. Hansma AH, Broxterman HJ, van der Horst I, Yuana Y, Boven E, Giaccone G, Pinedo HM, Hoekman K (2005) *Ann Oncol* 16:1695–1701.
7. Wedam SB, Low JA, Yang SX, Chow CK, Choyke P, Danforth D, Hewitt SM, Berman A, Steinberg SM, Liewehr DJ, *et al.* (2006) *J Clin Oncol* 24:769–777.
8. Marshall E (2002) *Science* 295:2198–2199.
9. Kunkel P, Ulbricht U, Bohlen P, Brockmann MA, Fillbrandt R, Stavrou D, Westphal M, Lamszus K (2001) *Cancer Res* 61:6624–6628.
10. O'Donnell A, Padhani A, Hayes C, Kakkar AJ, Leach M, Trigo JM, Scurr M, Raynaud F, Phillips S, Aherne W, *et al.* (2005) *Br J Cancer* 93:876–883.
11. Bouscary D, Legros L, Tulliez M, Dubois S, Mahe B, Boyne-Rausy O, Querre MC, Vassilief D, Varet B, Audoin A, *et al.* (2005) *Br J Haematol* 131:609–618.
12. Engebraaten O, Bjerkvig R, Pedersen PH, Laerum OD (1993) *Int J Cancer* 53:209–214.
13. Ignatova TN, Kukekov VG, Laywell ED, Suslov ON, Vrionis FD, Steindler DA (2002) *Glia* 39:193–206.
14. Dvorak P, Dvorakova D, Hampl A (2006) *FEBS Lett* 580:2869–2874.
15. Englund U, Fricker-Gates RA, Lundberg C, Bjorklund A, Wictorin K (2002) *Exp Neurol* 173:1–21.
16. Hurelbrink CB, Armstrong RJ, Dunnett SB, Rosser AE, Barker RA (2002) *Eur J Neurosci* 15:1255–1266.
17. Aboody KS, Brown A, Rainov NG, Bower KA, Liu S, Yang W, Small JE, Herrlinger U, Ourednik V, Black PM, *et al.* (2000) *Proc Natl Acad Sci USA* 97:12846–12851.
18. Visted T, Enger PO, Lund-Johansen M, Bjerkvig R (2003) *Front Biosci* 8:e289–304.
19. Brabletz T, Jung A, Spaderna S, Hlubek F, Kirchner T (2005) *Nat Rev Cancer* 5:744–749.
20. Holash J, Maisonpierre PC, Compton D, Boland P, Alexander CR, Zagzag D, Yancopoulos GD, Wiegand SJ (1999) *Science* 284:1994–1998.
21. Nasreen GN, Bender E, Zurakowski D, Kang SY, Sampson D, Flynn E, Watnick RS, Straume O, Akslen LA, Folkman J, Almog N (2006) *J Natl Cancer Inst* 98:316–325.
22. Carmeliet P (2005) *Oncology* 69 (Suppl 3):4–10.
23. Folkman J (1971) *N Engl J Med* 285:1182–1186.
24. Ribatti D (2005) *Br J Haematol* 128:303–309.
25. Ribatti D, Vacca A (2005) *Curr Cancer Drug Targets* 5:571–578.
26. Collins VP (2004) *J Neurol Neurosurg Psychiatry* 75 (Suppl 2):ii2–ii11.
27. Liu L, Backlund LM, Nilsson BR, Grander D, Ichimura K, Goike HM, Collins VP (2005) *J Mol Med* 83:917–926.
28. Karcher S, Steiner HH, Ahmadi R, Zoubaa S, Vasvari G, Bauer H, Unterberg A, Herold-Mende C (2006) *Int J Cancer* 118:2182–2189.
29. Kleihues P, Ohgaki H (1999) *Neuro-oncol* 1:44–51.
30. Engebraaten O, Hjortland GO, Hirschberg H, Fodstad O (1999) *J Neurosurg* 90:125–132.
31. Maheshparan R, Read TA, Lund-Johansen M, Skaftnesmo KO, Bjerkvig R, Engebraaten O (2003) *Acta Neuropathol (Berlin)* 105:49–57.
32. Shields AF, Grierson JR, Dohmen BM, Machulla HJ, Stayanoff JC, Lawhorn-Crews JM, Obradovich JE, Muzik O, Mangner TJ (1998) *Nat Med* 4:1334–1336.
33. Villa A, Snyder EY, Vescovi A, Martinez-Serrano A (2000) *Exp Neurol* 161:67–84.
34. Okabe M, Imai T, Kurusu M, Hiromi Y, Okano H (2001) *Nature* 411:94–98.
35. Schultz C, Lemke N, Ge S, Golembieski WA, Rempel SA (2002) *Cancer Res* 62:6270–6277.
36. Rich JN, Hans C, Jones B, Iversen ES, McLendon RE, Rasheed BK, Dobra A, Dressman HK, Bigner DD, Nevins JR, West M (2005) *Cancer Res* 65:4051–4058.
37. Shi Q, Bao S, Maxwell JA, Reese ED, Friedman HS, Bigner DD, Wang XF, Rich JN (2004) *J Biol Chem* 279:52200–52209.
38. Yuan X, Curtin J, Xiong Y, Liu G, Waschsmann-Hogiu S, Farkas DL, Black KL, Yu JS (2004) *Oncogene* 23:9392–9400.
39. Reya T, Morrison SJ, Clarke MF, Weissman IL (2001) *Nature* 414:105–111.
40. Marx J (2003) *Science* 301:1308–1310.
41. Singh SK, Clarke ID, Terasaki M, Bonn VE, Hawkins C, Squire J, Dirks PB (2003) *Cancer Res* 63:5821–5828.
42. Collins AT, Berry PA, Hyde C, Stower MJ, Maitland NJ (2005) *Cancer Res* 65:10946–10951.
43. Nakano I, Kornblum HI (2006) *Pediatr Res* 59:54R–58R
44. Bonnet D (2005) *Cell Prolif* 38:357–361.
45. Al-Hajj M, Wicha MS, Benito-Hernandez A, Morrison SJ, Clarke MF (2003) *Proc Natl Acad Sci USA* 100:3983–3988.
46. Singh SK, Hawkins C, Clarke ID, Squire JA, Bayani J, Hide T, Henkelman RM, Cusimano MD, Dirks PB (2004) *Nature* 432:396–401.
47. Bjerkvig R, Tysnes BB, Aboody KS, Najbauer J, Terzis AJ (2005) *Nat Rev Cancer* 5:899–904.
48. Blouw B, Song H, Tihan T, Bosze J, Ferrara N, Gerber HP, Johnson RS, Bergers G (2003) *Cancer Cell* 4:133–146.
49. Bjerkvig R, Tonnesen A, Laerum OD, Backlund EO (1990) *J Neurosurg* 72:463–475.
50. Wang J, Laschinger C, Zhao XH, Mak B, Sith A, McCulloch CA (2005) *Biochem Biophys Res Commun* 330:123–130.
51. Lin HJ, Hsieh FC, Song H, Lin J (2005) *Br J Cancer* 93:1372–1381.
52. Halvorsen OJ, Oyan AM, Bo TH, Olsen S, Rostad K, Haukaas SA, Bakke AM, Marzolf B, Dimitrov K, Stordrange L, *et al.* (2005) *Int J Oncol* 26:329–336.
53. Gjertsen BT, Oyan AM, Marzolf B, Hovland R, Gausdal G, Doskeland SO, Dimitrov K, Golden A, Kalland KH, Hood L, Bruserud O (2002) *J Hematother Stem Cell Res* 11:469–481.
54. Dysvik B, Jonassen I (2001) *Bioinformatics* 17:369–370.
55. Snijders AM, Nowak N, Segraves R, Blackwood S, Brown N, Conroy J, Hamilton G, Hindle AK, Huey B, Kimura K, *et al.* (2001) *Nat Genet* 29:263–264.